Cell Reports

Article

Early-Life Stress Regulates Cardiac Development through an IL-4-Glucocorticoid Signaling Balance

Graphical Abstract

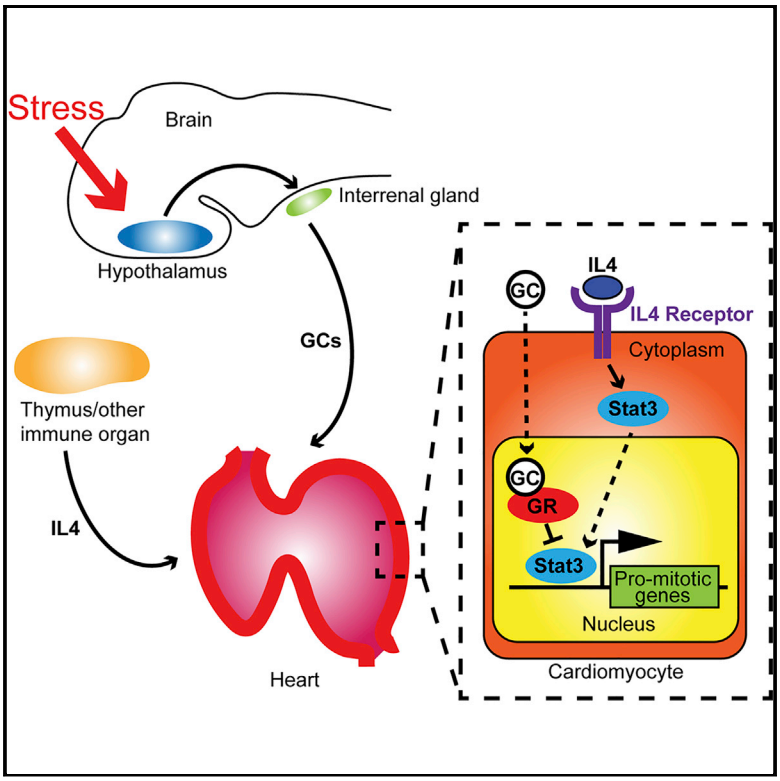

Authors

Dilem C. Apaydin,
Paul A. Morocho Jaramillo,
Laura Corradi, ..., Thomas Kammertoens,
Alessandro Filosa,
Suphansa Sawamiphak

Correspondence

suphansa.sawamiphak@mdc-berlin.de

In Brief

Apaydin et al. reveal molecular communications among stress, immune, and cardiovascular systems; provide evidence for the alteration of cardiac developmental program and adverse remodeling by early-life stress; and identify a cytokine signaling pathway mediating the modulation of cardiac development with the ability to counteract adverse stress response.

Highlights

- Early-life stress interferes with cardiac developmental program
- GR-IL-4 signaling interaction regulates cardiomyocyte proliferation
- GR and IL-4 act through regulation of Stat3 transcriptional activity
- GR and IL-4 functions in heart development are conserved in zebrafish and mouse

Apaydin et al., 2020, Cell Reports *33*, 108404
November 17, 2020 © 2020 The Author(s).
https://doi.org/10.1016/j.celrep.2020.108404

CellPress

Cell Reports

CellPress
OPEN ACCESS

Article

Early-Life Stress Regulates Cardiac Development through an IL-4-Glucocorticoid Signaling Balance

Dilem C. Apaydin,[1] Paul A. Morocho Jaramillo,[1] Laura Corradi,[1] Francesca Cosco,[1] Fritz G. Rathjen,[1] Thomas Kammertoens,[1,2] Alessandro Filosa,[1,4] and Suphansa Sawamiphak[1,3,4,5,*]
[1]Max Delbrück Center for Molecular Medicine, Robert-Rössle-Straße 10, 13092 Berlin, Germany
[2]Institute of Immunology, Charité Campus Berlin Buch, Lindenberger Weg 80, 13125 Berlin, Germany
[3]DZHK (German Center for Cardiovascular Research), Partner Site Berlin, Berlin, Germany
[4]These authors contributed equally
[5]Lead Contact
*Correspondence: suphansa.sawamiphak@mdc-berlin.de
https://doi.org/10.1016/j.celrep.2020.108404

SUMMARY

Stressful experiences early in life can increase the risk of cardiovascular diseases. However, it remains largely unknown how stress influences susceptibility to the disease onset. Here, we show that exposure to brain-processed stress disrupts myocardial growth by reducing cardiomyocyte mitotic activity. Activation of the glucocorticoid receptor (GR), the primary stress response pathway, reduces cardiomyocyte numbers, disrupts trabecular formation, and leads to contractile dysfunction of the developing myocardium. However, a physiological level of GR signaling is required to prevent cardiomyocyte hyperproliferation. Mechanistically, we identify an antagonistic interaction between the GR and the cytokine interleukin-4 (IL-4) as a key player in cardiac development. IL-4 signals transcription of key regulators of cell-cycle progression in cardiomyocytes via signal transducer and activator of transcription 3 (Stat3). GR, on the contrary, inhibits this signaling system. Thus, our findings uncover an interplay between stress and immune signaling pathways critical to orchestrating physiological growth of the heart.

INTRODUCTION

Substantial evidence suggests a strong association between early-life adversity and cardiovascular disease in adulthood (Kivimäki and Steptoe, 2018; Suglia et al., 2018). It has been proposed that early-life interventions targeting stress regulatory pathways may be more effective than treating downstream cardiovascular impairments after disease onset (Suglia et al., 2018). However, little is known about the causative role and mechanisms by which stress in early life affects the phenotypes of the cardiovascular system later.

In vertebrates, behavioral and physiological responses to stress are mainly orchestrated by the hypothalamus-pituitary-adrenal (HPA) axis (Chrousos and Gold, 1992). Within minutes of exposure to stressors, specialized hypothalamic neurons release the peptide corticotropin-releasing hormone (CRH) in the pituitary. Subsequent secretion of adrenocorticotropic hormone (ACTH) from the pituitary stimulates adrenal cortex production of glucocorticoids (GCs), the primary mediators of stress-responsive homeostasis in various organs (Chrousos and Gold, 1992; Sapolsky et al., 2000). The ability of GCs to alter neuroendocrine balance, metabolism, sympathetic activity, and immune function implies that systemic maladaptation to stress might underlie an increased susceptibility of the cardiovascular system to pathological onset (Kivimäki and Steptoe, 2018; Sapolsky et al., 2000; Suglia et al., 2018). Chronic inflammation, for example, has been reported in adults experiencing adversities in their childhood (Danese et al., 2007; Hostinar et al., 2015). However, HPA axis activation and GC production are strictly regulated by negative-feedback mechanisms to assure temporally restricted responses (Gjerstad et al., 2018; Osterlund et al., 2016), raising the question of how their effects persist into adulthood. Different hypotheses that have been proposed to explain the link between fetal exposure to excess GCs and increased risk for cardiovascular diseases later in life are based on indirect effects of stress on cardiac function (Braun et al., 2013; Tegethoff et al., 2009). Chronic elevation of blood pressure and other endocrine dysfunctions are among the major suspects to underlie adverse cardiometabolic events caused by modification of HPA axis functions (Braun et al., 2013; Tegethoff et al., 2009). Alternatively, other models link early-life stress to cardiovascular diseases through an intermediate role of stress-induced mental conditions, such as depression (Suglia et al., 2018). However, evidence demonstrating a causal relationship between early-life stress, and resulting behavioral or chronic hormonal disorders, and the irreversible maladaptation predisposing individuals to cardiovascular illness in adulthood is still lacking.

Although it was shown that GCs can alter the maturation of cardiomyocytes (CMs) (Oakley et al., 2013; Rog-Zielinska et al., 2015; Wilson et al., 2015), involvement of early-life stress signaling during development of the heart and molecular mechanisms underlying its actions are poorly understood. Here, we used physical,

This is an open access article under the CC BY-NC-ND license (http://creativecommons.org/licenses/by-nc-nd/4.0/).

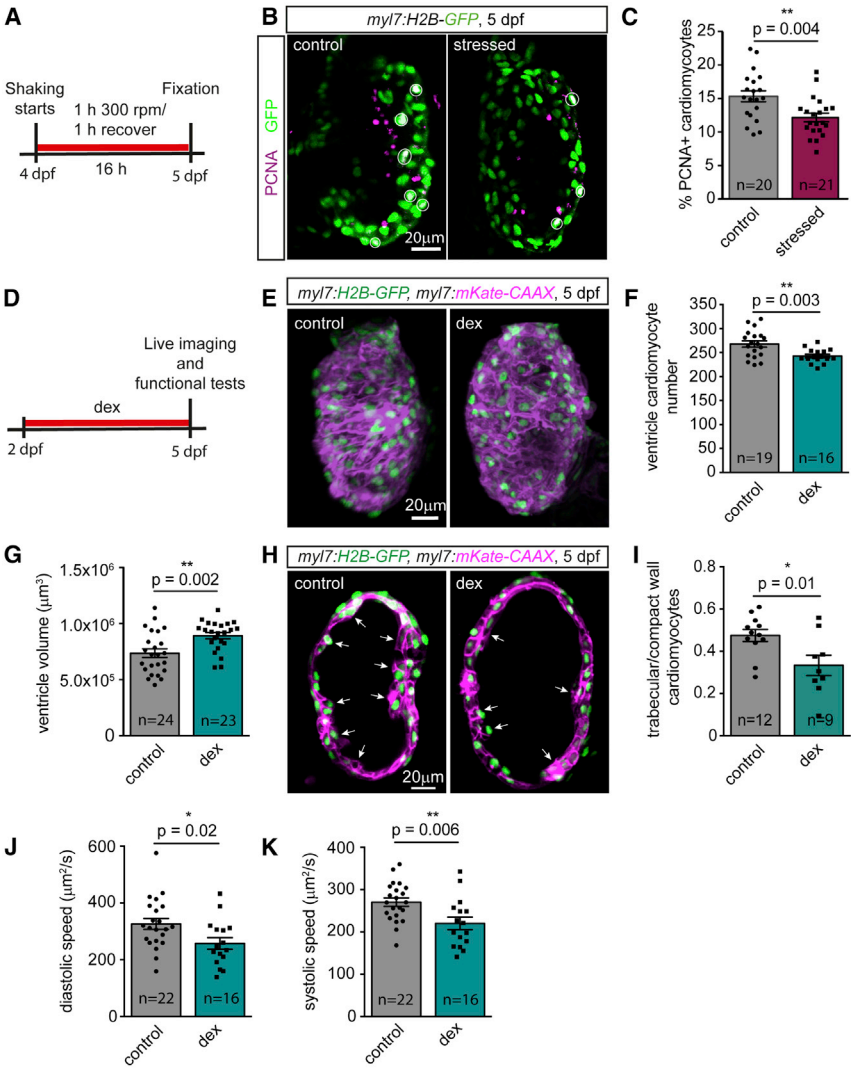

Figure 1. Exposure to Stress or Elevated GCs Reduces CM Proliferation, Lowers the Total Number of CMs, Impairs Trabeculation, and Attenuates Ventricular Contractility

(A) Scheme showing the timeline of vibrational stress application.

(B) The 5-dpf *Tg(myl7:H2B-GFP)*^{zf521} larval hearts after application of vibrational stress or control treatment, immunostained for the proliferation marker PCNA and GFP.

(C) Bar graph depicting the average percentage of PCNA-positive (PCNA^{+}) CMs in control and shaken (stressed) larvae.

(D) Schematic representation of the timeline for dex application.

(E) The 5-dpf *Tg(myl7:H2B-GFP)*^{zf521}; *Tg(myl7:mKate-CAAX)*^{sd11} control and dex-treated hearts.

(F and G) Graphs depicting average CM number (F) and ventricle volume (G) of control and dex-treated 5-dpf *Tg(myl7:H2B-GFP)*^{zf521}; *Tg(myl7:mKate-CAAX)*^{sd11} larvae.

(H) The 5-dpf *Tg(myl7:H2B-GFP)*^{zf521}; *Tg(myl7:mKate-CAAX)*^{sd11} hearts showing a reduced number of trabeculae (arrows) upon dex treatment.

(I) Graph showing reduced ratio of trabecular/compact wall CM numbers in dex-treated larvae compared to controls.

(J and K) Bar graphs showing diastolic (J) or systolic (K) speed of 5-dpf larval hearts treated with dex and controls.

Data are presented as mean ± SEM. *$p < 0.05$, **$p < 0.01$, t test. n indicates number of larvae used for experiments. See also Figures S1–S3.

pharmacological, and genetic perturbations of GC receptor (GR) signaling to test whether brain-mediated stress could directly influence the cardiac developmental program, resulting in early morphological and functional alterations of the heart. To this end, we exploited zebrafish to overcome the intrinsic difficulties related to experimental application of stressors in animals that develop *in utero*. We focused our attention on pre-hatching (2 to 3 days post-fertilization [dpf]) and early post-hatching periods (4 to 5 dpf) of zebrafish, when developmental stages of the heart are similar to late-gestational/early-postnatal ones in mammals. We revealed that stress negatively affects mitotic activity of CMs in the developing heart by affecting the transcription of key cell-cycle regulators. Importantly, we identified a stress-cytokine signaling interaction, in which GR counteracts pro-mitotic action of interleukin-4 (IL-4), to serve as an important regulator of myocardial growth. Together, our results uncover a role of stress signaling in cardiac development, reveal a non-immune signaling function of a cytokine, and identify an antagonistic interaction between these pathways in CMs.

RESULTS

Early-Life Stress Impairs CM Proliferation

First, to examine whether the cardiac developmental program is affected by brain-mediated stress triggered by a physical challenge experienced during early life, we exposed 4-dpf zebrafish larvae to a vibrational stimulus causing water shaking for 16 h (Figure 1A). This type of stimulus was previously employed to model a brain-mediated stress response in zebrafish larvae (Castillo-Ramírez et al., 2019). Interestingly, following this short-term exposure to the stressor, we observed a reduction of CM proliferation. In *Tg(myl7:H2B-GFP)*^{zf521} larvae, in which CM nuclei were fluorescently marked by histone-H2B-tagged GFP (H2B-GFP; Figure 1B), a decreased mitotic rate was detectable by immunostaining of proliferating cell nuclear antigen (PCNA), labeling nuclei of cells in the G1-S phase (Figures 1B and 1C). Thus, a physical challenge inducing brain-processed stress causes an anti-mitotic response in CMs during cardiac morphogenesis.

Activation of the GR Reduces CM Numbers, Disrupts Trabeculation, and Impairs Contractility of the Developing Myocardium

HPA-axis-induced GC production activates diverse cellular responses to stress by binding to the GR. While GCs are key

"stress hormones," pleiotropic effects of GC-activated GR can be unrelated to stress response. On the other hand, stress response could be GR independent (MacDougall-Shackleton et al., 2019). To test whether brain-mediated stress imposes its developmental perturbation effect on the heart through GR activation, we used the potent GR agonist dexamethasone (dex). Physiologically, embryos of placental mammals are exposed to negligible levels of GCs, but endogenous GCs rise rapidly at late gestation (Fowden et al., 1998; Rog-Zielinska et al., 2015). Therefore, we chose to examine the effect of dex from 2 dpf in zebrafish to recapitulate the late gestation developmental stage of the heart (Andrés-Delgado and Mercader, 2016).

Upon 3-day dex treatment from 2 dpf to 5 dpf (Figure 1D), the cardiac ventricle contained fewer CMs, as observed from the expression of nuclear GFP and membrane mKate in CMs of *Tg(myl7:H2B-GFP)*^{zf521}*; Tg(myl7:mKate-CAAX)*^{sd11} larvae (Figures 1E and 1F). The reduction of CM number was not a result of increased cell death. As in control siblings, dex-treated larvae showed a negligible number of CMs undergoing apoptosis (Figure S1A). Further examination of the ventricular wall revealed eccentric hypertrophy, characterized by increased ventricular volume (Figures 1E and 1G) and caused at least in part by hypertrophic growth of CMs (Figure S1B). Trabeculation—a critical developmental process closely associated with CM proliferation, which allows an increase of muscle mass for proper contractile function—was disrupted by dex treatment (Figures 1H and 1I). By contrast, development of the endocardium and epicardium was not affected by dex treatment (Figures S2A–S2D), suggesting that the action of GC signaling in the developing heart is restricted to the myocardium. As a consequence of myocardial morphological alterations, dex-treated hearts displayed attenuated functionality, as evidenced by reduced diastolic and systolic speed (Figures 1J and 1K; Videos S1 and S2). No significant reduction of ejection fraction or fractional shortening was observed following 3-day dex treatment (Figures S3A and S3B), suggesting that the dex-induced reduction of CM numbers might not be associated with myocardial stiffening, a common hallmark of the transition from compensated hypertrophy to heart failure (Makarenko et al., 2004). Taken together, these data suggest that stress influences heart development through the anti-proliferative action of the GR in CMs, leading to adverse morphological and functional alteration of the myocardium.

IL-4 Signaling Regulates CM Mitosis during Development

Upon binding to the GR, GCs induce pleiotropic effects on various cell types by direct binding to DNA via GC response element or interaction with other transcription factors to regulate gene transcription (Cain and Cidlowski, 2017). One of the most widely appreciated roles of GCs is their potent immune suppressive property. Crosstalk between GCs and immunomodulatory pathways such as pattern recognition and cytokine signaling underlies the ability of GCs to promote inflammatory resolution and inhibit leukocyte activation (Cain and Cidlowski, 2017). In addition, expression of different cytokines—including IL-4, IL-6, IL-17, and interferon (IFN)γ—in certain immune cell types is regulated by GCs (Cain and Cidlowski, 2017). Moreover, phenotypical and functional alterations of immune cells have been proposed to underlie adverse cardiovascular remodeling (Swirski and Nahrendorf, 2018). For these reasons, we hypothesized that dysregulation of immune pathways by excessive GR activation might mediate the effect of stress on morphological and functional remodeling of the developing heart. In search of a potential mediator of GR-immune crosstalk in the heart, we first focused on cytokine signaling. *In situ* hybridization showed that a cognate receptor of the signature cytokine of the type II inflammatory response, IL-4 receptor (IL-4r), was expressed in CMs of the developing zebrafish heart as early as 3 dpf (Figure S4A). We could not detect *il4* mRNA in the heart, but it was prominently expressed at a close proximity in the thymus, a hematopoietic organ (Figures S4B and S4C), suggesting that as in mammals, IL-4 is mainly produced by immune cells also in zebrafish larvae. We also examined expression of the principal type I pro-inflammatory cytokine IFNγ and its receptor but found them to be undetectable in the myocardium (Figures S4D and S4E). Interestingly, IL-4 abundance was reported to be inversely correlated with anxiety (Hou et al., 2017), a mental condition associated with stress. Cardiac tissue expression and relation to stress of this cytokine/receptor system prompted us to examine further its role in cardiac development and crosstalk with GR signaling.

First, we generated the transgenic line *Tg(hsp70:il4-6xHIS)*^{md74} that enables heat-inducible expression of 6xHIS-tagged IL-4 (*il4-6xHIS*) under control of the 70 kilodalton heat shock protein (hsp70) promoter (Figure 2A). To understand the effect of excessive IL-4 production in the developing heart, we examined *Tg(hsp70:il4-6xHIS)*^{md74}*; Tg(myl7:H2B-GFP)*^{zf521}*; Tg(myl7:mKate-CAAX)*^{sd11} larvae following heat induction of *il4-6xHIS* overexpression daily from 1 to 5 dpf (Figure 2B). Larvae exposed to elevated IL-4 levels showed a higher number of ventricular CMs and increased ventricular volume (Figures 2C–2E). Formation of the trabecular layer was not altered by IL-4 induction, as shown by comparable ratios of trabecular/compact wall CMs (Figures 2F and 2G). Development of the endocardium and the epicardium was also not affected (Figures S2E–S2H). The overgrowth of the heart was associated with increased diastolic and systolic speed (Figures 2H and 2I; Videos S3 and S4) but did not alter ejection fraction and fractional shortening (Figures S3C and S3D). Thus, morphological and functional characterizations indicate that supplemental CMs observed upon *il4-6xHIS* overexpression integrated normally into the myocardium and improved cardiac contractility.

Our findings on IL-4 induction of myocardial overgrowth prompted further investigation of the requirement of IL-4 signaling to regulate CM mitotic rate. To this end, we assessed proliferation rate of 5-dpf *Tg(myl7:H2B-GFP)*^{zf521} larvae at 16 h following pericardial injection of an IL-4-neutralizing antibody (Figure 2J), previously shown to efficiently antagonize IL-4 action in zebrafish (Bhattarai et al., 2016). PCNA immunohistochemistry showed that IL-4 deficiency caused a reduction of CM proliferation in 5-dpf larvae, compared to siblings injected with control antibody against a 6-histidine epitope (Figures 2K and 2L).

Taken together, these gain- and loss-of-function approaches identify a previously unknown function of the cytokine IL-4 as an indispensable regulator for cardiac development through the control of CM proliferation.

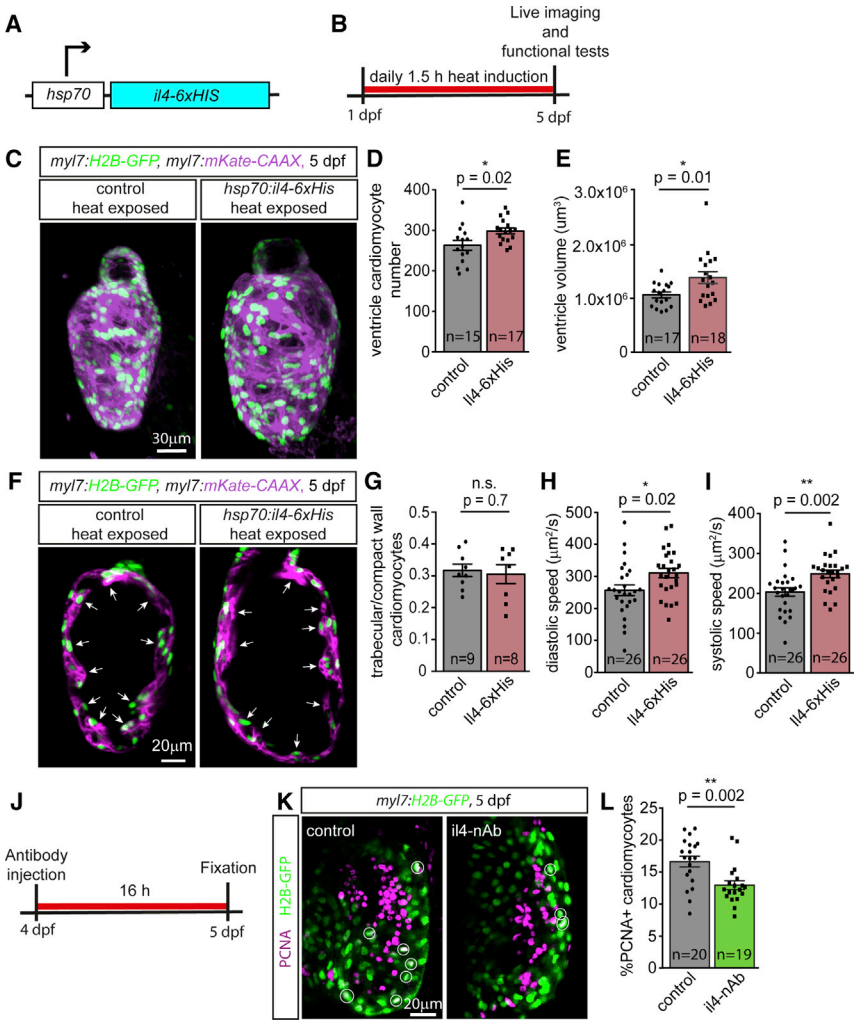

Figure 2. IL-4 Induces Myocardial Growth and Improves Ventricular Contractile Function

(A) Scheme of the *hsp70:il4-6xHIS* transgenic construct.

(B) Diagram illustrating design of the *il4-6xHis* overexpression experiment.

(C) Hearts of 5-dpf control *Tg(myl7:H2B-GFP)^{zf521}; Tg(myl7:mKate-CAAX)^{sd11}* and *il4-6xHis*-overexpressing *Tg(hsp70:il4-6xHIS)^{md74}; Tg(myl7:H2B-GFP)^{zf521}; Tg(myl7:mKate-CAAX)^{sd11}* larvae. CM nuclei and membranes are labeled with H2B-GFP and mKate-CAAX, respectively.

(D and E) Bar graphs showing average ventricle CM number (D) and ventricle volume (E) of control and *il4-6xHis*-overexpressing 5-dpf larvae.

(F) Normal formation of trabeculae (arrows) in 5-dpf control and *il4-6xHis*-overexpressing *Tg(myl7:H2B-GFP)^{zf521}; Tg(myl7:mKate-CAAX)^{sd11}* larvae.

(G) Bar graph showing similar ratios of trabecular/compact wall CM numbers in *il4-6xHIS*-overexpressing and control larvae.

(H and I) Bar graphs displaying average diastolic (H) and systolic (I) speeds of 5-dpf *Tg(hsp70:il4-6xHIS)^{md74}; Tg(myl7:H2B-GFP)^{zf521}; Tg(myl7:mKate-CAAX)^{sd11}* larval hearts.

(J) Scheme of the loss-of-function experiment design.

(K) The 5-dpf *Tg(myl7:H2B-GFP)^{zf521}* hearts of larvae injected with antibody against IL-4 (il4-nAB) or against 6x-His repetitive sequence as control.

(L) Bar graph depicting average percentage of PCNA-positive (PCNA$^+$) CMs in 5-dpf *Tg(myl7:H2B-GFP)^{zf521}* larvae injected with IL-4-nAB and control antibodies.

Data are presented as mean ± SEM. *$p < 0.05$, **$p < 0.01$, n.s., not significant, t test. n indicates number of larvae used for experiments. See also Figures S2–S4.

GC Interacts with IL-4 Signaling Pathway Independently of *il4* or *il4r* Transcriptional Control

To test whether GC and IL-4 signaling pathways interact with each other to regulate heart development, we performed PCNA analysis to assess CM proliferation in *Tg(myl7:H2B-GFP)^{zf521}* larvae exposed to combinatorial manipulations of both pathways (Figures 3A–3C). Consistent with our finding of an anti-mitotic effect of stress (Figures 1B and 1C), 6 h of dex exposure reduced ventricular CM proliferation in 5-dpf larvae (Figures 3B and 3C). Having shown that GCs act as a CM mitotic brake, we next asked whether GC signaling only mediates developmental adaptation of the heart in response to stress or if it might play a role in physiological growth. Intriguingly, contrary to the mitotic suppression in response to GR activation, GR inhibition by 6 h of treatment with the drug mifepristone (mif) was able to drive a higher percentage of CMs into the cell cycle compared to control siblings (Figures 3B and 3C). Similarly, we observed an increase of CM proliferation at 6 h after induction of *il4-6xHIS* expression (Figures 3B and 3C), further supporting the pro-mitotic role of IL-4. Importantly, dex-mediated GR activation abolished the effect of *il4-6xHIS* overexpression (Figures 3B and 3C), indicating the interaction between the two pathways. Similar responses to activation of IL-4 and GR pathways were also observed in atrial CMs, indicating that the role of IL-4-GR signaling interaction as a proliferative regulator is not limited to the ventricle (Figure S5).

Since GCs can inhibit the transcription of various cytokines (Cain and Cidlowski, 2017), we next tested whether suppression of *il4* or *il4r* expression might underlie the antagonistic interaction between the GR and IL-4 pathways. However, qPCR analyses showed that GR activation by dex treatment did not alter levels of whole-body *il4* mRNA and cardiac IL-4 receptor complex *il4r*, *il13ra1*, and *il13a2* mRNAs (Figure 4A). These observations indicate that GR regulates CM proliferation by a different mechanism involving interaction with IL-4 downstream signaling.

GCs and IL-4 Act Upstream of Stat3 to Balance Mitotic Activity in CMs

A key mediator of IL-4 signaling is the transcription factor Stat6 (Kelly-Welch et al., 2005). IL-4 binding to the IL-4r leads to Stat6 activation and subsequent expression of several IL-4 target genes. To gain further mechanistic insight into how GCs

CellPress
OPEN ACCESS

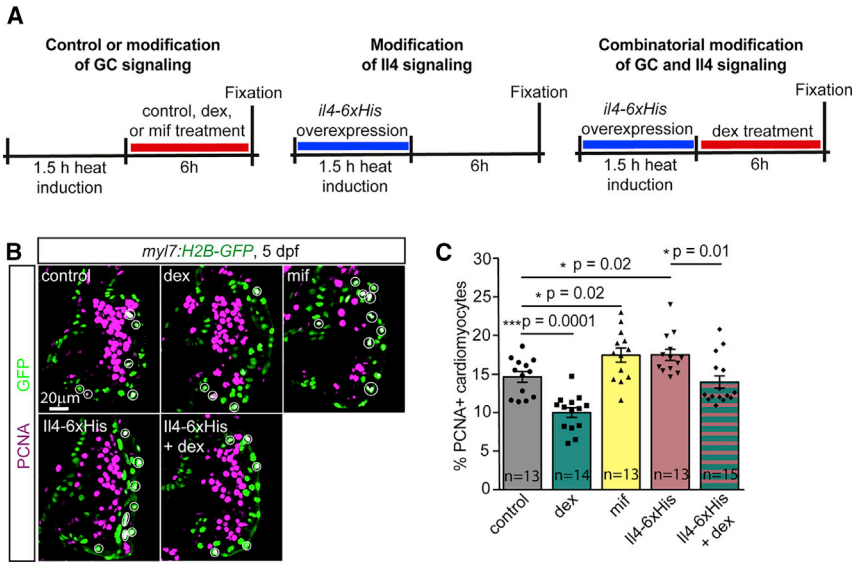

Figure 3. GR and IL-4 Signaling Interact to Regulate Cardiac Development

(A) Schemes showing timeline of drug treatment (red bars) and heat induction of *il4-6xHis* expression (blue bars).

(B) Images of 5-dpf *Tg(myl7:H2B-GFP)*^{zf521} cardiac ventricles following control treatment (control), dex treatment (dex) and mif-treatment (mif), or *Tg(hsp70:il4-6xHIS)*^{md74}; *Tg(myl7:H2B-GFP)*^{zf521} hearts after *il4-6xHis* overexpression (IL-4-6xHis) and simultaneous *il4-6xHis* overexpression and dex treatment (IL-4-6xHis + dex), stained with antibodies against PCNA and GFP.

(C) Bar graph depicting average percentage of PCNA^{+} ventricular CMs in 5-dpf larvae exposed to different combinations of *il4-6xHis* overexpression and GR signaling inhibition (mif) or activation (dex).

Data are presented as mean ± SEM. *$p < 0.05$, ***$p < 0.001$, t test. n indicates number of larvae used for experiments. See also Figure S5.

and IL-4 interact to control CM proliferation, we first tested whether the expression of Stat6 transcriptional targets involved in cell division is altered in the developing heart upon IL-4 and GC signaling activation. While the Stat6 target genes *bcl2l1* and *socs1a* were readily upregulated at 2 h after *il4-6xHis* overexpression, their expression was unaltered by dex-induced GR activation (Figures 4B and 4C). Thus, we next examined the expression of genes controlled by the transcription factor Stat3, also activated by IL-4 (Rahaman et al., 2005). In agreement with the antagonistic effect of GCs and IL-4 in CM proliferation (Figure 3C), 2 h of dex treatment reduced, while *il4-6xHis* overexpression increased, expression of the Stat3-targeted pro-mitotic genes *c-myc* and *cyclind1* in the cardiac tissue (Figures 4D and 4E). Expression of *gata3*, another Stat3-regulated gene involved in cell proliferation, was reduced by dex treatment but not significantly increased by *il4-6xHis* overexpression (Figure 4F). Expression of *stat3* itself was not altered by dex treatment (Figure S6). From this regulatory role of both GCs and IL-4 on Stat3 target genes, we hypothesized that the two signaling pathways regulate CM mitotic activity through modulation of Stat3 activation and thus transcription of genes governing cell-cycle progression.

To test this hypothesis, we employed a well-characterized dominant-negative form of Stat3 (DNStat3), carrying a tyrosine-to-phenylalanine mutation in the activation loop that inhibits endogenous Stat3 signaling by competing with its receptor interaction (Conway, 2006) (Figures 4G–4L). Inducible expression of DNStat3 specifically in CMs was achieved by treatment of *Tg(myl7:H2B-GFP)*^{zf521}; *Tg(myl7:creER)*^{pd10}; *Tg(actb2:loxP-DsRed-loxP-DNStat3-GFP)*^{pd59} embryos with 4-hydroxytamoxifen (4-OHT) from 1 to 2 dpf (Figure 4G). Analysis of PCNA content at 5 dpf showed that DNStat3 reduced the CM proliferative rate compared to control siblings (Figures 4H and 4I). Importantly, DNStat3 also abolished the increase of the proliferative rate induced by overexpression of *il4-6xHis* (Figures 4H and 4I), indicating that Stat3 is a crucial mediator of IL-4 mitogenic signaling in CMs. Furthermore, expression of DNStat3 in CMs abolished the pro-mitotic effect of mif-mediated GR inhibition (Figures 4J–4L). Together, these data indicate that IL-4 and GC antagonistic signaling through regulation of Stat3 activity in CMs fine-tunes cell proliferation not only in response to stressors, but also during physiological development of the heart.

Cell-Autonomous Signaling by the GR and IL-4r in CMs Regulates Their Proliferation

GCs are known to modulate growth hormone secretion (Mazziotti and Giustina, 2013), raising the possibility that their effect on CM proliferation might be secondary to a reduction of overall growth rate. However, disruption of cell proliferation by modulation of Stat3 activity specifically in CMs suggests cell-autonomous signaling of the GR and IL-4r. To test this hypothesis, we generated a transgenic construct to express the GR specifically in CMs. The construct harboring a *mKate-GR* fusion transgene, linked by a polypeptide linker and placed downstream of the *myl7* promoter (Figure 5A), was injected into 1–2 cell-stage *Tg(myl7:H2B-GFP)*^{zf521} embryos to achieve mosaic expression. Analysis of PCNA contents 5 days later showed that a significantly lower percentage of mKate-GR^{+} CMs entered the cell cycle as compared to mKate-GR^{-} cells in the same hearts (Figures 5D–5G and 5P), confirming the role of the GR in antagonizing mitotic signaling in CMs. Importantly, these findings also suggest that elevated GCs in response to stress suppress mitotic activity directly through activation of the GR present in CMs and not indirectly through growth hormone secretion.

To interfere with endogenous IL-4r signaling in CMs, we injected into 1–2 cell-stage embryos a construct encoding *myl7*-driven *Il4r* with its cytoplasmic domain truncated and fused to the red fluorescent protein (*Il4rΔC-RFP*; Figure 5B). The truncated form lacking the cytoplasmic domain containing the Stat docking site was shown to interfere with the endogenous IL-4r to activate Stat-mediated gene expression (Gandhi et al., 2014). In line with our finding of the requirement of IL-4 signaling

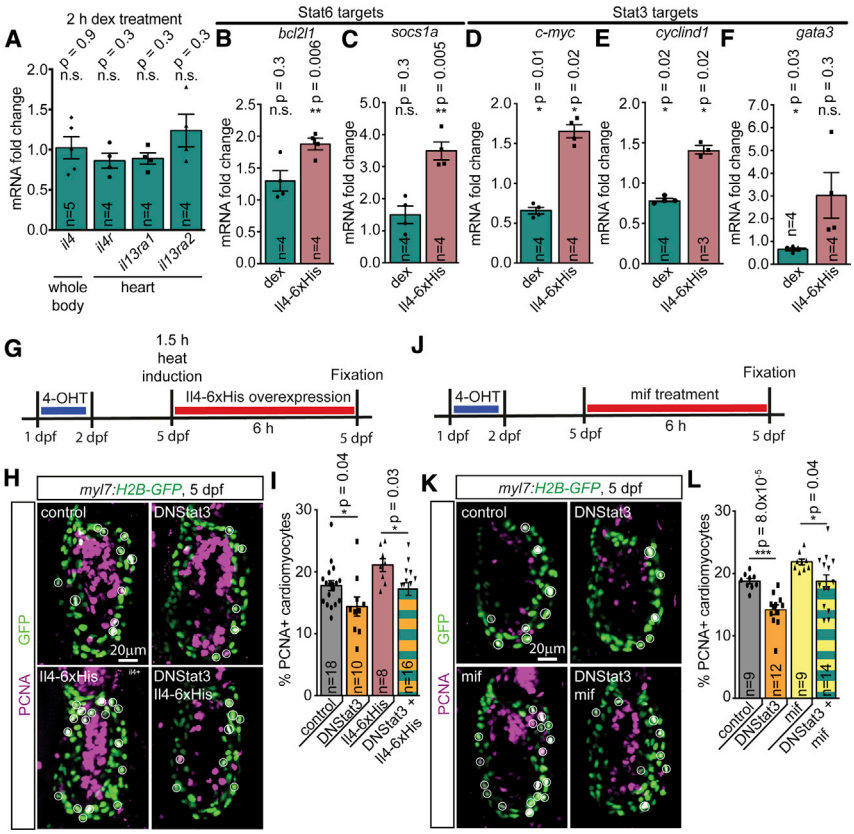

Figure 4. Regulation of Myocardial Growth by GR and IL-4 Signaling Interaction Is Mediated by Stat3

(A) Bar graphs showing average fold changes of mRNA encoding IL-4 and its receptors IL-4r, IL-13ra1, and IL-13ra2 in 5-dpf larvae treated with dex for 2 h.

(B–F) Graphs depicting average fold change of mRNA transcribed from genes downstream of Stat6 (B and C) or Stat3 (D–F) in the hearts of 5-dpf wild-type larvae exposed to dex or *il4-6xHIS*-overexpressing *Tg(hsp70:il4-6xHIS)*^{md74} larvae.

(G) Schematic representation of experimental design to obtain data shown in (H) and (I). CM-specific expression of *creER* in *Tg(myl7:H2B-GFP)*^{zf521}; *Tg(myl7:creER)*^{pd10}; *Tg(actb2:loxP-DsRed-loxP-DNStat3-GFP)*^{pd59} embryos was induced with 4-OHT treatment from 1 to 2 dpf. Overexpression of *Il4-6xHis* from the *hsp70:il4-6xHis* transgene was induced by exposure to 38°C for 1.5 h.

(H) The 5-dpf control and DNStat3-expressing hearts with and without *il4-6xHis* overexpression, immunostained for PCNA and GFP.

(I) Bar graph depicting average percentages of PCNA$^+$ CMs in control, *DNStat3*-overexpression, *il4-6xHis*-overexpression, and *il4-6xHis* + *DNStat3*-overexpression treatment groups.

(J) Design of experiment shown in (K) and (L). *DNStat3* expression was induced as described in (G). The GR inhibitor mif was applied at 5 dpf for 6 h before sample fixation.

(K) PCNA and GFP immunostaining of 5-dpf control and *DNStat3*-expressing hearts with and without mif treatment.

(L) Bar graph showing average percentages of PCNA$^+$ CMs in control, mif treatment, *DNStat3*-overexpression, and *DNStat3*-overexpression with mif treatment groups.

Data are presented as mean ± SEM. *p < 0.05, **p < 0.01, ***p < 0.001, n.s., not significant, t test. n indicates number of samples of pooled hearts or larvae (A–F) or number of larvae (I and L). See also Figure S6.

in CM proliferation, assessment of PCNA expression showed that mitotic rates of Il4rΔC-RFP$^+$ CMs were lower than those of Il4rΔC$^-$ cells in 5-dpf hearts (Figures 5H–5K and 5Q). In larvae injected with a control *myl7:RFP* plasmid, proliferation rates of RFP$^+$ and RFP$^-$ CMs were similar (Figures 5C, 5L–5O, and 5R). The *myl7:mKate-GR*, *myl7:Il4rΔC-RFP*, and *myl7:RFP* plasmids did not induce cell death, since cells expressing the constructs were not stained with TUNEL (Figure S7A), and we did not detect reduced numbers of CMs expressing the transgenes between 3 and 5 dpf (Figure S7B).

Together these data strongly suggest that CM-autonomous GR and IL-4r signaling interacts through Stat3, which is negatively regulated by GR and acts as positive relay for the IL-4r.

IL-4Ra Is Indispensable for CM Proliferation in the Developing Mouse Heart

In order to address the question of if the role of IL-4 signaling in heart development is evolutionary conserved, we measured the proliferative rate of CMs in the neonatal heart of mice harboring a null mutation of the *IL-4 receptor alpha* (*Il4ra*) gene. Immunostaining of the cell proliferation marker Ki67—expressed during G1-M phases—in sections of hearts of P0 *Il4ra*$^{-/-}$ mice revealed a lower proliferation rate of CMs, identified with immunofluorescent staining of the CM marker Troponin T2 (Tnnt2), compared to control *Il4ra*$^{+/+}$ animals (Figures 6A and 6B). Proliferation rate was also reduced in *Il4ra*$^{+/-}$ hearts, although it was still significantly higher than that of *Il4ra*$^{-/-}$ mutants. Accordingly, membrane labeling of CMs by wheat germ agglutinin (WGA) indicated lower CM density in *Il4ra*$^{-/-}$ and, to a lesser extent, in *Il4ra*$^{+/-}$ hearts (Figures 6C and 6D). CMs in *Il4ra*$^{-/-}$ mice were larger than in *Il4ra*$^{+/+}$ controls (Figure 6E), suggesting that the developing heart might compensate for the presence of fewer CMs upon IL-4Ra loss with hypertrophic growth. In contrast, lack of IL-4Ra did not alter CMs ploidy (Figures 6F and 6G). Moreover, hearts of *Il4ra*$^{+/-}$ and *Il4ra*$^{-/-}$ mice did not show gross morphological alteration nor increased fibrosis (Figures 6H and 6I), suggesting the requirement of IL-4 signaling specifically in CM proliferation, but not in other cardiac morphogenesis processes. These data strongly suggest an important evolutionary conserved role of IL-4 signaling in controlling the development of vertebrate hearts.

GC-IL-4 Signaling Regulates Proliferation of Mouse CMs

Next, we asked if the interaction between the GC and IL-4 signaling pathways we observed in zebrafish also occurs in mice. To this end, we quantified proliferation of cultured CMs

CellPress
OPEN ACCESS

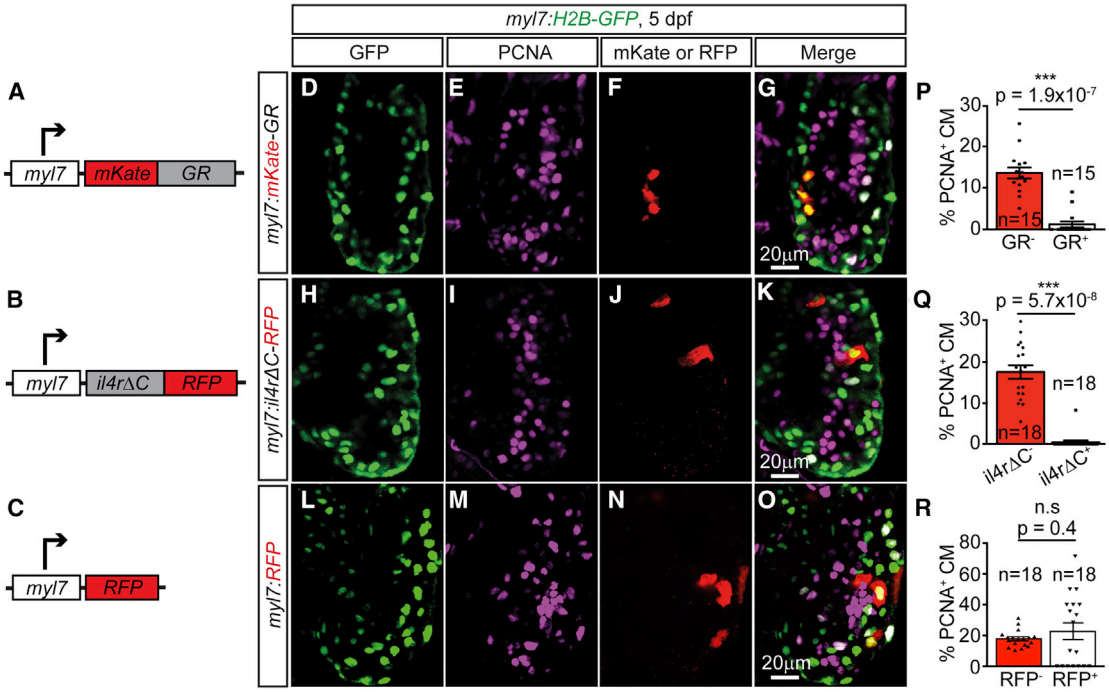

Figure 5. GR and IL-4r Signaling Regulate CM Proliferation Cell Autonomously

(A–C) Schemes of the transgenic constructs used in the experiment displayed in (D)–(R).

(D–O) Confocal images depicting ventricles of 5-dpf *Tg(myl7:H2B-GFP)*^{zf521} fish injected at 1–2 cell stages with plasmids containing *myl7:mKate-GR* (D–G), *myl7:il4rΔC-RFP* (H–K), or *myl7:RFP* (L–O) transgenes.

(P–R) Graphs depicting percentages of PCNA$^+$ CMs either containing or not containing the mKate-GR (P) or Il4rΔC-RFP (Q) recombinant proteins or RFP (R). Data are presented as mean ± SEM. ***p < 0.001, n.s., not significant, t test. n indicates number of larvae used for experiments. See also Figure S7.

obtained from neonatal (P0) mice after activation of GC and/or IL-4 pathways (Figure 7). In agreement with our results in zebrafish, 24 h of dex treatment after 2 days in culture reduced CM proliferation—assessed with incorporation of the thymidine analog 5-Ethynyl-2′-deoxyuridine (EdU) applied for 12 h—compared to control. In contrast, application of recombinant IL-4 for 24 h resulted in higher percentages of CMs entering the cell cycle. Similar to what we observed *in vivo* in zebrafish, activation of GC signaling with dex antagonized the mitogenic effect of IL-4.

These results indicate that the modulatory role of GC-IL-4 signaling interaction on CM proliferation is an evolutionarily conserved feature among different vertebrates.

DISCUSSION

Excessive or precocious exposure to GCs in early life retards overall growth and increases the risk of cardiovascular disease observed in adulthood (Seckl and Holmes, 2007). In the heart, it was shown that GCs act via the GR to promote structural maturation of the myocardium in mouse and zebrafish (Rog-Zielinska et al., 2013; Wilson et al., 2015). Mice lacking the GR in CMs spontaneously develop hypertrophic cardiomyopathy and die prematurely from heart failure (Oakley et al., 2013). These studies used pharmacological or genetic interventions (i.e., application of exogenous GCs or mutagenesis of the GR) to interfere with stress-responsive pathways. Here, we show that brain-mediated stress triggered by a physical challenge (forceful alteration of swimming pattern) early in life has a strong influence on cardiac development.

Our work has revealed a regulatory function of GR signaling in CM proliferation. Excessive GR signaling disrupts physiological growth of the myocardium through suppression of CM cell division, leading to underdeveloped trabecular layer, cardiac hypertrophic remodeling, and contractile dysfunction. The antiproliferative response of CMs and subsequent alteration of myocardial morphology might be a mechanism by which stress regulates developmental programming. Consequently, detrimental outcomes of functional alteration may culminate in cardiovascular pathology later in life. The negative impact of GR activation on contraction and relaxation speeds, but insignificant effects on ejection fraction and fractional shortening of the ventricle, imply an adaptive response of the developing heart. Accordingly, eccentric hypertrophy, commonly associated with fewer ventricular CM numbers (Tracy, 2013), occurred upon GR activation. This morphological alteration is known to predispose the heart to failure risk, particularly systolic dysfunction (Gjesdal et al., 2011; Kuroda, 2015; Velagaleti et al., 2014).

Our finding that inhibition of GR signaling leads to myocardial hyperproliferation is surprising, given the common assumption that the stress response occurring in late development (Seckl and Holmes, 2007) only plays a role in CM maturation (Oakley

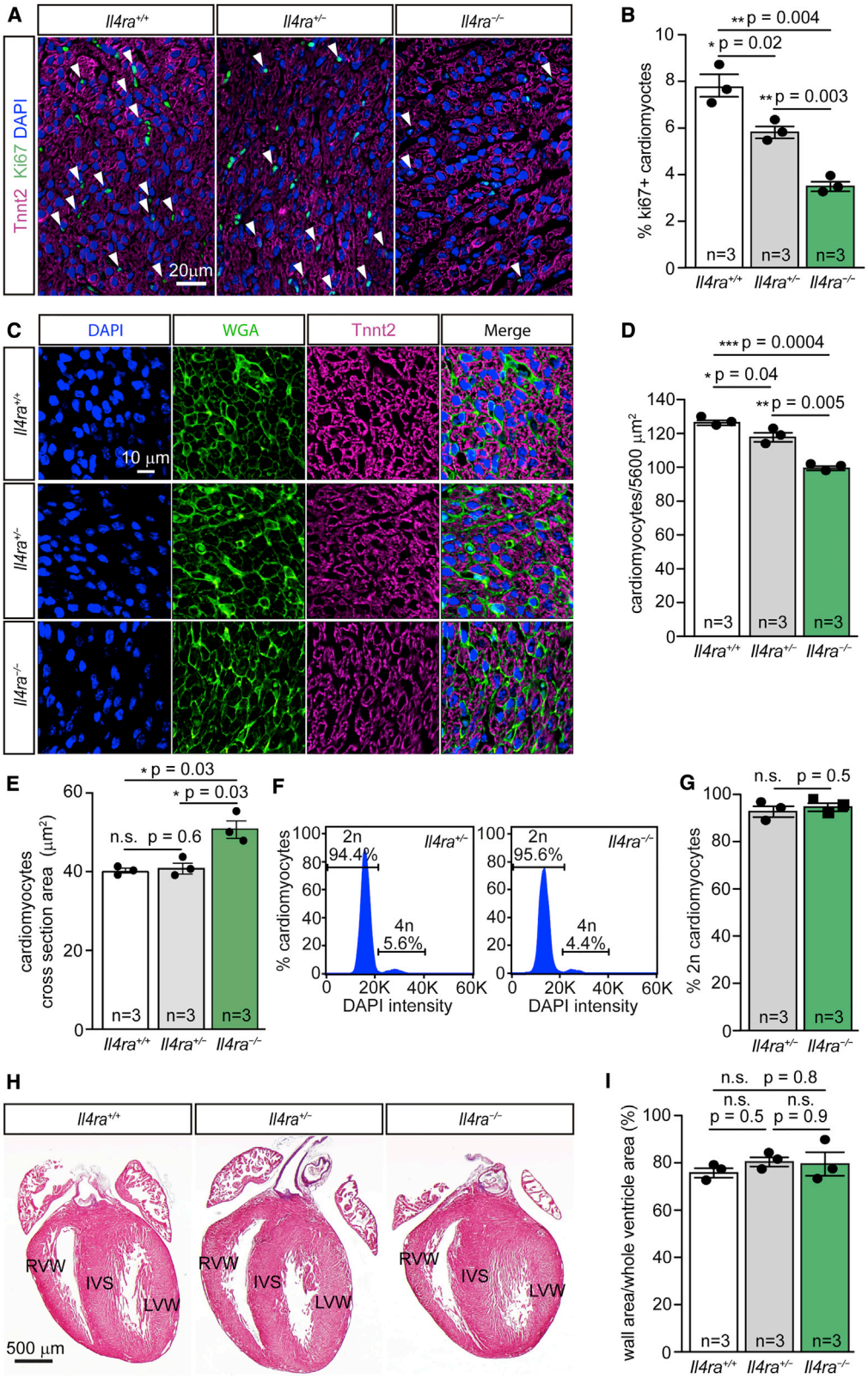

(legend on next page)

et al., 2013; Rog-Zielinska et al., 2013). In fact, significantly elevated left ventricular mass has been observed in CM-specific GR knockout mice in the absence of fibrosis and prior to activation of hypertrophic response (Oakley et al., 2013), suggesting the possible occurrence of myocardial hyperplasia and its causative role in these morphological and functional adversities. Our finding calls for a better understanding of the functional implications of GR signaling in the physiological development of the heart, extending beyond the current model implicating it only as an adaptive response to stress. The balance of GR activity might regulate a trade-off between proliferation and maturation of CMs that, if perturbed, may reduce resilience to heart disease in adulthood. Our findings reveal that finetuning the level of GR signaling activation is, at least in part, mediated by an inter-organ signaling crosstalk, involving the brain (HPA axis), the heart (GR and IL-4r activation in CMs), and possibly the immune system (IL-4 production) and orchestrating a competitive GR-IL-4 interaction to activate Stat3. By interfering with the GR, IL-4r, and Stat3 activation specifically in CMs, we showed that the signaling interaction acts directly in these muscle cells, and it is not due to indirect effects mediated by other cell types. These manipulations did not lead to death or evident morphological alterations of CMs, suggesting their specificity in modulating proliferation, although other possible subtle alterations of cell physiology cannot be completely excluded.

Cytokines can act both locally and systemically through their secretion by tissue-resident or recruited immune cells and diffusion into circulation (Assen and Sixt, 2017; Perona-Wright et al., 2010). Despite their accessibility to virtually all tissues and broad biological responses, we still know little about non-immune roles of cytokine signaling pathways. IL-4 is best known as an inducer of Th2 response (Chen et al., 2004). It was reported that in steady state, in the absence of infection, mice produce small quantities of IL-4 that can be detected in the serum (Finkelman and Morris, 1999). In addition to immune cells, IL-4 was shown to be secreted from developing skeletal muscles to attract myoblast recruitment to promote fusion and growth (Horsley et al., 2003). In the adult heart, IL-4 might exhibit a pro-fibrotic role. IL-4 deficiency was linked to reduced interstitial collagen production in response to hypertension, protecting the heart from adverse functional remodeling (Kanellakis et al., 2012; Peng et al., 2015). Here, we report a previously unrecognized role of IL-4 as a pro-mitotic signal for CMs of the developing heart acting through the atypical signaling transducer Stat3. This function appears to be evolutionarily conserved in vertebrates, since we observed its requirement and interaction with the GC signaling pathway in both zebrafish and mouse. The fact that IL-4 is known to be secreted by immune cells, together with our data showing strong expression of *il4* in the thymus of zebrafish larvae, suggests that the source of IL-4 acting on heart development may be cells of the immune system. However, with the tools used in this work, we could not pinpoint a direct role of immune-cells-derived IL-4 in cardiac development. An approach using cell-type-specific loss-of-function of *il4* will be required to unambiguously prove an involvement of the immune system. The GC and IL-4 signaling interaction identified here differs from the well-known immunosuppressive action of corticosteroids through inhibition of cytokine production (Cain and Cidlowski, 2017). We did not detect changes in the expression of IL-4 signaling molecules including the ligand itself, its receptors, or *stat3* in response to alteration of GR signaling. Instead, we showed that a fine balance of GR and IL-4 signaling regulates CM Stat3 activation and thereby transcriptional activity of several Stat3 target genes that serve as key mediators of the cell-cycle machinery. While the stress response—through activation of the GR—leads to suppression of CM proliferation, at the cost of morphological alteration and contractile dysfunction, GR activity may be required to maintain physiological growth rate of the myocardium by balancing the level of activated Stat3 in CMs. On the other hand, IL-4 could counterbalance GR hyperactivation and restore CM mitotic activity through competitive activation of Stat3. In line with our finding, Stat3 has been shown to play a key role in cell-cycle reentry of matured mammalian CMs, a hallmark of cardiac regeneration (Miyawaki et al., 2017). Thus, our work suggests that activated Stat3 represents a potential target for the prevention/reversion of cell-cycle exit and terminal differentiation of CMs upon exposure to early-life stress.

STAR★METHODS

Detailed methods are provided in the online version of this paper and include the following:

- KEY RESOURCES TABLE
- RESOURCE AVAILABILITY
  - Lead Contact
  - Materials Availability
  - Data and Code Availability

Figure 6. Mice Lacking IL-4Ra Exhibit Low CM Proliferative Rate and Reduced CM Density, but Normal Gross Heart Morphology and Lack of Fibrosis

(A) P0 heart sections from *Il4ra*$^{+/+}$, *Il4ra*$^{+/-}$, and *Il4ra*$^{-/-}$ mice, stained for the CM marker Tnnt2, the proliferation marker Ki67, and DAPI.

(B) Graph depicting the average percentage of Ki67^{+} CMs in P0 *Il4ra*$^{+/+}$, *Il4ra*$^{+/-}$, and *Il4ra*$^{-/-}$ mice.

(C) Images showing WGA, Tnnt2, and DAPI staining of sections from P0 *Il4ra*$^{+/+}$, *Il4ra*$^{+/-}$, and *Il4ra*$^{-/-}$ hearts.

(D) Graph depicting average WGA^{+}/Tnnt2^{+} CM density.

(E) Graph depicting average CM size, measured as cell cross-section area.

(F) Representative plots showing distribution of DAPI fluorescence intensities in fluorescence-activated cell sorting (FACS)-sorted CMs from a *Il4ra*$^{+/-}$ and a *Il4ra*$^{-/-}$ heart. The fluorescence intensity ranges used for determining diploid (2n) and tetraploid (4n) cells are indicated by the horizontal bars.

(G) Graph showing average percentage of diploid (2n) CMs in *Il4ra*$^{+/-}$ and *Il4ra*$^{-/-}$ hearts.

(H) Sections from P0 *Il4ra*$^{+/+}$, *Il4ra*$^{+/-}$, and *Il4ra*$^{-/-}$ hearts stained with Masson's trichrome method, showing lack of fibrosis in *Il4ra*$^{+/-}$ and *Il4ra*$^{-/-}$ hearts. RVW, right ventricular wall; LVW, left ventricular wall; IVS, intra-ventricular septum.

(I) Graph showing average ventricular wall thickness (quantified as percentage of wall area in total ventricle area).

Data are presented as mean ± SEM. *$p < 0.05$, **$p < 0.01$, ***$p < 0.001$, n.s., not significant, t test. n indicates number of mice used for experiments.

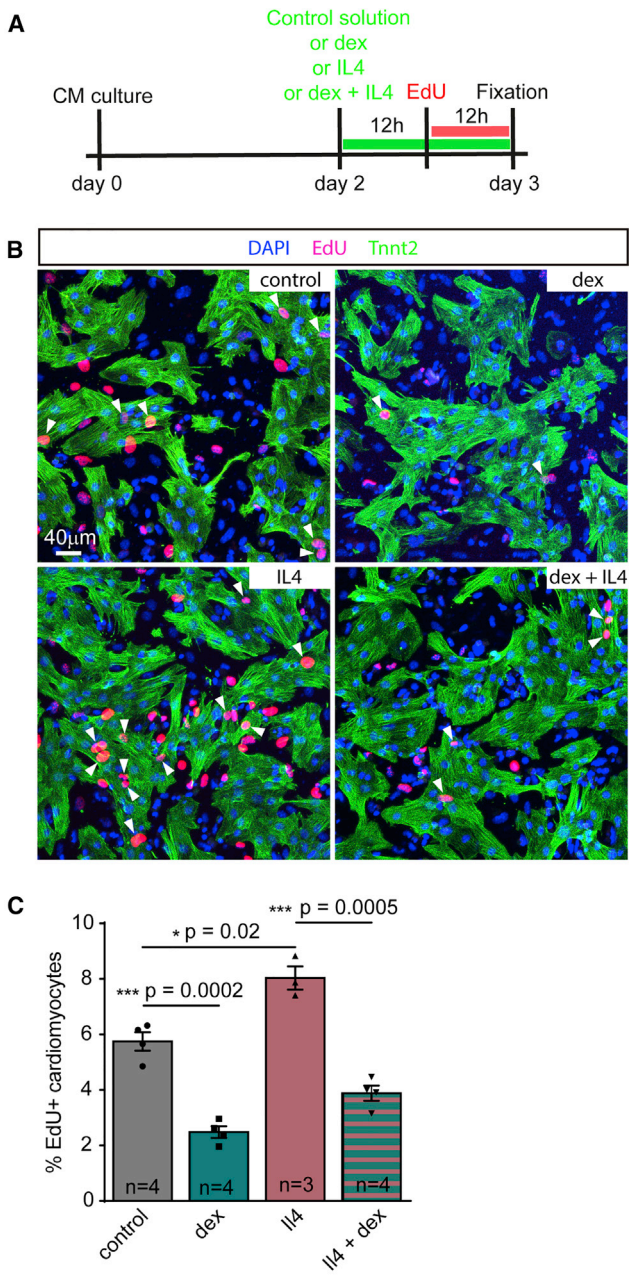

Figure 7. GR and IL-4 Signaling Interact to Regulate Proliferation of Mouse CMs.

(A) Schemes showing timeline of control, dex, IL-4 (green bar), and EdU (red bar) treatments.

(B) Images of cultured neonatal (P0) mouse CMs treated with control solution, dex, IL-4, and dex plus IL-4 combinatorial exposure. CMs were immunostained with an antibody against Tnnt2 (green). Proliferating cells were labeled by DNA incorporation of EdU (purple), and cell nuclei were stained with DAPI (blue).

(C) Bar graph depicting average percentage of EdU^+ CMs exposed to different combinations of GR (dex) and IL-4 signaling activation.

Data are presented as mean ± SEM. *$p < 0.05$, ***$p < 0.001$, t test. n indicates number of biological replicates.

- EXPERIMENTAL MODEL AND SUBJECT DETAILS
  - Zebrafish
  - Mice
- METHOD DETAILS
  - Generation of expression constructs
  - Gene expression by heat-induction and treatments with drug and neutralizing antibody
  - Stress treatment
  - Immunofluorescent and TUNEL staining
  - Image analyses
  - Mouse histological and immunofluorescence analyses
  - *In situ* hybridization
  - Cardiac contractility measurements
  - Real-time PCR
- PRIMERS USED IN THE EXPERIMENT ARE
  - Mouse cardiomyocyte isolation, culture and immunocytochemistry
  - Flow cytometry and polyploidy analysis
- QUANTIFICATION AND STATISTICAL ANALYSIS

SUPPLEMENTAL INFORMATION

Supplemental Information can be found online at https://doi.org/10.1016/j.celrep.2020.108404.

ACKNOWLEDGMENTS

The authors would like to acknowledge technical support from A. Banerjee, F. Oadri, C. Friese, I. Duckert, the staff of the Zebrafish Facility, and the Advanced Light Microscopy Technology Platform at the Max Delbrück Center for Molecular Medicine. We are thankful to M. Schaaf for providing us with a plasmid containing the zebrafish GR coding sequence. This work was supported by the Helmholtz Association of German Research Centres (project ID number VH-NG-1247).

AUTHOR CONTRIBUTIONS

S.S. and A.F. conceived and designed experiments, provided supervision, and administered the project. D.C.A. designed and performed experiments. F.C., F.G.R., P.A.M.J., L.C., S.S., and A.F. performed experiments. T.K. provided resources and support for mouse experiments. D.C.A., F.C., P.A.M.J., S.S., and A.F. analyzed data. S.S. and A.F. wrote the manuscript. All authors commented on the manuscript.

DECLARATION OF INTERESTS

The authors declare no competing interests.

Received: May 8, 2020
Revised: September 21, 2020
Accepted: October 27, 2020
Published: November 17, 2020

REFERENCES

Andrés-Delgado, L., and Mercader, N. (2016). Interplay between cardiac function and heart development. Biochim. Biophys. Acta *1863*, 1707–1716.

Assen, F.P., and Sixt, M. (2017). The Dynamic Cytokine Niche. Immunity *46*, 519–520.

Bhattarai, P., Thomas, A.K., Cosacak, M.I., Papadimitriou, C., Mashkaryan, V., Froc, C., Reinhardt, S., Kurth, T., Dahl, A., Zhang, Y., and Kizil, C. (2016). IL4/STAT6 Signaling Activates Neural Stem Cell Proliferation and Neurogenesis upon Amyloid-β42 Aggregation in Adult Zebrafish Brain. Cell Rep. *17*, 941–948.

Braun, T., Challis, J.R., Newnham, J.P., and Sloboda, D.M. (2013). Early-life glucocorticoid exposure: the hypothalamic-pituitary-adrenal axis, placental function, and long-term disease risk. Endocr. Rev. *34*, 885–916.

Burns, C.G., Milan, D.J., Grande, E.J., Rottbauer, W., MacRae, C.A., and Fishman, M.C. (2005). High-throughput assay for small molecules that modulate zebrafish embryonic heart rate. Nat. Chem. Biol. *1*, 263–264.

Cain, D.W., and Cidlowski, J.A. (2017). Immune regulation by glucocorticoids. Nat. Rev. Immunol. *17*, 233–247.

Castillo-Ramírez, L.A., Ryu, S., and De Marco, R.J. (2019). Active behaviour during early development shapes glucocorticoid reactivity. Sci. Rep. *9*, 12796–12799.

Chen, L., Grabowski, K.A., Xin, J.-P., Coleman, J., Huang, Z., Espiritu, B., Alkan, S., Xie, H.B., Zhu, Y., White, F.A., et al. (2004). IL-4 induces differentiation and expansion of Th2 cytokine-producing eosinophils. J. Immunol. *172*, 2059–2066.

Chi, N.C., Shaw, R.M., De Val, S., Kang, G., Jan, L.Y., Black, B.L., and Stainier, D.Y.R. (2008). Foxn4 directly regulates tbx2b expression and atrioventricular canal formation. Genes Dev. *22*, 734–739.

Chrousos, G.P., and Gold, P.W. (1992). The concepts of stress and stress system disorders. Overview of physical and behavioral homeostasis. JAMA *267*, 1244–1252.

Conway, G. (2006). STAT3-dependent pathfinding and control of axonal branching and target selection. Dev. Biol. *296*, 119–136.

Danese, A., Pariante, C.M., Caspi, A., Taylor, A., and Poulton, R. (2007). Childhood maltreatment predicts adult inflammation in a life-course study. Proc. Natl. Acad. Sci. USA *104*, 1319–1324.

Davison, J.M., Akitake, C.M., Goll, M.G., Rhee, J.M., Gosse, N., Baier, H., Halpern, M.E., Leach, S.D., and Parsons, M.J. (2007). Transactivation from Gal4-VP16 transgenic insertions for tissue-specific cell labeling and ablation in zebrafish. Dev. Biol. *304*, 811–824.

Fang, Y., Gupta, V., Karra, R., Holdway, J.E., Kikuchi, K., and Poss, K.D. (2013). Translational profiling of cardiomyocytes identifies an early Jak1/Stat3 injury response required for zebrafish heart regeneration. Proc. Natl. Acad. Sci. USA *110*, 13416–13421.

Finkelman, F.D., and Morris, S.C. (1999). Development of an assay to measure in vivo cytokine production in the mouse. Int. Immunol. *11*, 1811–1818.

Fowden, A.L., Li, J., and Forhead, A.J. (1998). Glucocorticoids and the preparation for life after birth: are there long-term consequences of the life insurance? Proc. Nutr. Soc. *57*, 113–122.

Fu, J., Gao, J., Pi, R., and Liu, P. (2005). An optimized protocol for culture of cardiomyocyte from neonatal rat. Cytotechnology *49*, 109–116.

Gandhi, H., Worch, R., Kurgonaite, K., Hintersteiner, M., Schwille, P., Bökel, C., and Weidemann, T. (2014). Dynamics and interaction of interleukin-4 receptor subunits in living cells. Biophys. J. *107*, 2515–2527.

Gibson, U.E., Heid, C.A., and Williams, P.M. (1996). A novel method for real time quantitative RT-PCR. Genome Res. *6*, 995–1001.

Gjerstad, J.K., Lightman, S.L., and Spiga, F. (2018). Role of glucocorticoid negative feedback in the regulation of HPA axis pulsatility. Stress *21*, 403–416.

Gjesdal, O., Bluemke, D.A., and Lima, J.A. (2011). Cardiac remodeling at the population level–risk factors, screening, and outcomes. Nat. Rev. Cardiol. *8*, 673–685.

Gray, C., Loynes, C.A., Whyte, M.K.B., Crossman, D.C., Renshaw, S.A., and Chico, T.J.A. (2011). Simultaneous intravital imaging of macrophage and neutrophil behaviour during inflammation using a novel transgenic zebrafish. Thromb. Haemost. *105*, 811–819.

Heckel, E., Boselli, F., Roth, S., Krudewig, A., Belting, H.G., Charvin, G., and Vermot, J. (2015). Oscillatory Flow Modulates Mechanosensitive klf2a Expression through trpv4 and trpp2 during Heart Valve Development. Curr. Biol. *25*, 1354–1361.

Horsley, V., Jansen, K.M., Mills, S.T., and Pavlath, G.K. (2003). IL-4 acts as a myoblast recruitment factor during mammalian muscle growth. Cell *113*, 483–494.

Hostinar, C.E., Lachman, M.E., Mroczek, D.K., Seeman, T.E., and Miller, G.E. (2015). Additive contributions of childhood adversity and recent stressors to inflammation at midlife: Findings from the MIDUS study. Dev. Psychol. *51*, 1630–1644.

Hou, R., Garner, M., Holmes, C., Osmond, C., Teeling, J., Lau, L., and Baldwin, D.S. (2017). Peripheral inflammatory cytokines and immune balance in Generalised Anxiety Disorder: Case-controlled study. Brain Behav. Immun. *62*, 212–218.

Kanellakis, P., Ditiatkovski, M., Kostolias, G., and Bobik, A. (2012). A profibrotic role for interleukin-4 in cardiac pressure overload. Cardiovasc. Res. *95*, 77–85.

Kelly-Welch, A., Hanson, E.M., and Keegan, A.D. (2005). Interleukin-4 (IL-4) pathway. Sci. STKE *2005*, cm9.

Kikuchi, K., Holdway, J.E., Werdich, A.A., Anderson, R.M., Fang, Y., Egnaczyk, G.F., Evans, T., Macrae, C.A., Stainier, D.Y.R., and Poss, K.D. (2010). Primary contribution to zebrafish heart regeneration by gata4(+) cardiomyocytes. Nature *464*, 601–605.

Kivimäki, M., and Steptoe, A. (2018). Effects of stress on the development and progression of cardiovascular disease. Nat. Rev. Cardiol. *15*, 215–229.

Kuroda, K. (2015). Hypertensive cardiomyopathy: A clinical approach and literature review. WJH *5*, 41–52.

Lin, Y.-F., Swinburne, I., and Yelon, D. (2012). Multiple influences of blood flow on cardiomyocyte hypertrophy in the embryonic zebrafish heart. Dev. Biol. *362*, 242–253.

MacDougall-Shackleton, S.A., Bonier, F., Romero, L.M., and Moore, I.T. (2019). Glucocorticoids and "Stress" Are Not Synonymous. Integr. Organismal Biol. *1*, obz017.

Makarenko, I., Opitz, C.A., Leake, M.C., Neagoe, C., Kulke, M., Gwathmey, J.K., del Monte, F., Hajjar, R.J., and Linke, W.A. (2004). Passive stiffness changes caused by upregulation of compliant titin isoforms in human dilated cardiomyopathy hearts. Circ. Res. *95*, 708–716.

Mazziotti, G., and Giustina, A. (2013). Glucocorticoids and the regulation of growth hormone secretion. Nat. Rev. Endocrinol. *9*, 265–276.

Mickoleit, M., Schmid, B., Weber, M., Fahrbach, F.O., Hombach, S., Reischauer, S., and Huisken, J. (2014). High-resolution reconstruction of the beating zebrafish heart. Nat. Methods *11*, 919–922.

Miyawaki, A., Obana, M., Mitsuhara, Y., Orimoto, A., Nakayasu, Y., Yamashita, T., Fukada, S.-I., Maeda, M., Nakayama, H., and Fujio, Y. (2017). Adult murine cardiomyocytes exhibit regenerative activity with cell cycle reentry through STAT3 in the healing process of myocarditis. Sci. Rep. *7*, 1407.

Noben-Trauth, N., Shultz, L.D., Brombacher, F., Urban, J.F., Jr., Gu, H., and Paul, W.E. (1997). An interleukin 4 (IL-4)-independent pathway for CD4+ T cell IL-4 production is revealed in IL-4 receptor-deficient mice. Proc. Natl. Acad. Sci. USA *94*, 10838–10843.

Oakley, R.H., Ren, R., Cruz-Topete, D., Bird, G.S., Myers, P.H., Boyle, M.C., Schneider, M.D., Willis, M.S., and Cidlowski, J.A. (2013). Essential role of stress hormone signaling in cardiomyocytes for the prevention of heart disease. Proc. Natl. Acad. Sci. USA *110*, 17035–17040.

Osterlund, C.D., Rodriguez-Santiago, M., Woodruff, E.R., Newsom, R.J., Chadayammuri, A.P., and Spencer, R.L. (2016). Glucocorticoid Fast Feedback Inhibition of Stress-Induced ACTH Secretion in the Male Rat: Rate Independence and Stress-State Resistance. Endocrinology *157*, 2785–2798.

Peng, H., Sarwar, Z., Yang, X.-P., Peterson, E.L., Xu, J., Janic, B., Rhaleb, N., Carretero, O.A., and Rhaleb, N.-E. (2015). Profibrotic Role for Interleukin-4 in Cardiac Remodeling and Dysfunction. Hypertension *66*, 582–589.

Perner, B., Englert, C., and Bollig, F. (2007). The Wilms tumor genes wt1a and wt1b control different steps during formation of the zebrafish pronephros. Dev. Biol. *309*, 87–96.

Perona-Wright, G., Mohrs, K., and Mohrs, M. (2010). Sustained signaling by canonical helper T cell cytokines throughout the reactive lymph node. Nat. Immunol. *11*, 520–526.

Rahaman, S.O., Vogelbaum, M.A., and Haque, S.J. (2005). Aberrant Stat3 signaling by interleukin-4 in malignant glioma cells: involvement of IL-13Ralpha2. Cancer Res. *65*, 2956–2963.

Rog-Zielinska, E.A., Thomson, A., Kenyon, C.J., Brownstein, D.G., Moran, C.M., Szumska, D., Michailidou, Z., Richardson, J., Owen, E., Watt, A., et al. (2013). Glucocorticoid receptor is required for foetal heart maturation. Hum. Mol. Genet. *22*, 3269–3282.

Rog-Zielinska, E.A., Craig, M.-A., Manning, J.R., Richardson, R.V., Gowans, G.J., Dunbar, D.R., Gharbi, K., Kenyon, C.J., Holmes, M.C., Hardie, D.G., et al. (2015). Glucocorticoids promote structural and functional maturation of foetal cardiomyocytes: a role for PGC-1α. Cell Death Differ. *22*, 1106–1116.

Sapolsky, R.M., Romero, L.M., and Munck, A.U. (2000). How do glucocorticoids influence stress responses? Integrating permissive, suppressive, stimulatory, and preparative actions. Endocr. Rev. *21*, 55–89.

Sawamiphak, S., Kontarakis, Z., and Stainier, D.Y.R. (2014). Interferon gamma signaling positively regulates hematopoietic stem cell emergence. Dev. Cell *31*, 640–653.

Sawamiphak, S., Kontarakis, Z., Filosa, A., Reischauer, S., and Stainier, D.Y.R. (2017). Transient cardiomyocyte fusion regulates cardiac development in zebrafish. Nat. Commun. *8*, 1525.

Schaaf, M.J.M., Champagne, D., van Laanen, I.H.C., van Wijk, D.C.W.A., Meijer, A.H., Meijer, O.C., Spaink, H.P., and Richardson, M.K. (2008). Discovery of a functional glucocorticoid receptor β-isoform in zebrafish. Endocrinology *149*, 1591–1599.

Seckl, J.R., and Holmes, M.C. (2007). Mechanisms of disease: glucocorticoids, their placental metabolism and fetal 'programming' of adult pathophysiology. Nat. Clin. Pract. Endocrinol. Metab. *3*, 479–488.

Suglia, S.F., Koenen, K.C., Boynton-Jarrett, R., Chan, P.S., Clark, C.J., Danese, A., Faith, M.S., Goldstein, B.I., Hayman, L.L., Isasi, C.R., et al.; American Heart Association Council on Epidemiology and Prevention; Council on Cardiovascular Disease in the Young; Council on Functional Genomics and Translational Biology; Council on Cardiovascular and Stroke Nursing; and Council on Quality of Care and Outcomes Research (2018). Childhood and Adolescent Adversity and Cardiometabolic Outcomes: A Scientific Statement From the American Heart Association. Circulation *137*, e15–e28.

Swirski, F.K., and Nahrendorf, M. (2018). Cardioimmunology: the immune system in cardiac homeostasis and disease. Nat. Rev. Immunol. *18*, 733–744.

Tegethoff, M., Pryce, C., and Meinlschmidt, G. (2009). Effects of intrauterine exposure to synthetic glucocorticoids on fetal, newborn, and infant hypothalamic-pituitary-adrenal axis function in humans: a systematic review. Endocr. Rev. *30*, 753–789.

Tracy, R.E. (2013). Eccentric may differ from concentric left ventricular hypertrophy because of variations in cardiomyocyte numbers. J. Card. Fail. *19*, 517–522.

Velagaleti, R.S., Gona, P., Pencina, M.J., Aragam, J., Wang, T.J., Levy, D., D'Agostino, R.B., Lee, D.S., Kannel, W.B., Benjamin, E.J., and Vasan, R.S. (2014). Left ventricular hypertrophy patterns and incidence of heart failure with preserved versus reduced ejection fraction. Am. J. Cardiol. *113*, 117–122.

Wilson, K.S., Baily, J., Tucker, C.S., Matrone, G., Vass, S., Moran, C., Chapman, K.E., Mullins, J.J., Kenyon, C., Hadoke, P.W.F., and Denvir, M.A. (2015). Early-life perturbations in glucocorticoid activity impacts on the structure, function and molecular composition of the adult zebrafish (Danio rerio) heart. Mol. Cell. Endocrinol. *414*, 120–131.

Yalcin, H.C., Amindari, A., Butcher, J.T., Althani, A., and Yacoub, M. (2017). Heart function and hemodynamic analysis for zebrafish embryos. Dev. Dyn. *246*, 868–880.

CellPress
OPEN ACCESS

STAR★METHODS

KEY RESOURCES TABLE

REAGENT or RESOURCE	SOURCE	IDENTIFIER
Antibodies		
monoclonal mouse anti human IL4 antibody	R&D systems	Cat# MAB204; RRID: AB_2126745
monoclonal mouse 6X-HIS antibody	Invitrogen	Cat# MA1-21315; RRID: AB_557403
polyclonal chick anti-GFP	Thermo Fisher	Cat# A10262; RRID: AB_2534023
polyclonal rabbit RFP	MBL	Cat# PM005; RRID: AB_591279
monoclonal mouse Anti-Proliferating Cell Nuclear Antigen (PCNA)	Dako	Cat# M0879; RRID: AB_2160651
monoclonal mouse anti cardiac Troponin T2	Abcam	Cat# ab33589; RRID: AB_727035
polyclonal rabbit Anti-Ki-67 Antibody	Millipore	Cat# AB9260; RRID: AB_2142366
Alexa Fluor 488 Anti-chicken	Thermo Fisher	Cat# A-11039; RRID: AB_142924
Alexa Fluor 647 Anti-mouse	Cell Signaling	Cat# 4410S; RRID: AB_1904023
Alexa Fluor 555 Anti-rabbit	Cell Signaling	Cat# 4413; RRID: AB_10694110
Alexa Fluor 488 Anti-rabbit	Cell Signaling	Cat# 4412; RRID: AB_1904025
Alexa Fluor 488 Anti-mouse	Cell Signaling	Cat# 4408S; RRID: AB_10694704
Biological Samples		
Cardiomyocytes from P0 C57BL/6N mice	MDC animal facility	N/A
Chemicals, Peptides, and Recombinant Proteins		
Wheat germ agglutinin-conjugated CF555	Biotium	Cat# 29076-1
Dexamethasone	Sigma	Cat# D1756
Miferpristone	Sigma	Cat# M8046
4-hydroxytamoxifen (4-OHT)	Sigma	Cat# H7904
TRIzol	Life Technologies	Cat# 15596026
Trypsin-EDTA	Sigma	Cat# T4049
Trypsin	GIBCO	Cat# 15090046
DNaseI	Roche	Cat# 10104159001
Dulbecco's Modified Eagle Medium, high glucose, GlutaMAX	GIBCO	Cat# 31966021
Fetal Bovine Serum	GIBCO	Cat# 10270106
Penicillin-Streptomycin (10.000 U/ml)	Thermo Fisher	Cat# 15140122
Fibronectin Bovine Protein, Plasma	Thermo Fisher	Cat# 33010-018
dexamethasone- suitable for cell culture	Sigma	Cat# D4902
recombinant murine IL4	PeproTech	Cat# 214-14
Liberase TL Research Grade	Roche	Cat# 5401020001
Pluron F-68 polyol, 100 ml	MP Biomedicals	Cat# 092750049
Critical Commercial Assays		
Click-iT EdU imaging kit	Thermo Fisher	Cat# C10640
Click-iT TUNEL Alexa Fluor 647	Thermo Fisher	Cat# C10247
Masson's trichrome staining kit	Roche	Cat# 860-031
Cold Fusion Cloning Kit	System Biosciences	Cat# MC010A-1
SuperScript III First Strand Kit	Life Technologies	Cat# 18080051
Luna Universal qPCR Master Mix	New England BioLabs	Cat# M3003
Experimental Models: Organisms/Strains		
Zebrafish: *Tg(myl7:Cre-ERT2)*^{pd12}	Kikuchi et al., 2010	ZFIN: ZDB-ALT-110307-1
Zebrafish: *Tg(myl7:mKate-CAAX)*^{sd11}	Lin et al., 2012	ZFIN: ZDB-ALT-120320-1
Zebrafish: *Tg(myl7:H2B-GFP)*^{zf521}	Mickoleit et al., 2014	ZFIN: ZDB-ALT-071120-1

(*Continued on next page*)

Continued

REAGENT or RESOURCE	SOURCE	IDENTIFIER
Zebrafish: *Tg(actb2:loxP-DsRed-loxP-dnstat3 EGFP)*^{s928}	Fang et al., 2013	ZFIN: ZDB-ALT-110210-11
Zebrafish: *Tg(myl7:GAL4)*^{s740}	Sawamiphak et al., 2017	ZFIN: ZDB-ALT-180427-1
Zebrafish: *Tg(myl7:GFP)*^{f1}	Burns et al., 2005	ZFIN: ZDB-ALT-060719-2
Zebrafish: *TgBAC(csf1ra:GAL4-VP16)*^{i186}	Gray et al., 2011	ZFIN: ZDB-ALT-110707-2
Zebrafish: *Tg(UAS-E1B:NTR-mCherry)*^{c264}	Davison et al., 2007	ZFIN: ZDB-ALT-070316-1
Zebrafish: *Tg(kdrl:Hsa.HRAS-mCherry)*^{s896}	Chi et al., 2008	ZFIN: ZDB-ALT-081212-4
Zebrafish: *Tg(fli:nls-mcherry)*^{ubs10}	Heckel et al., 2015	ZFIN: ZDB-ALT-160726-2
Zebrafish: *Tg(wt1b:EGFP)*^{li1}	Perner et al., 2007	ZFIN: ZDB-ALT-071127-1
Zebrafish: *Tg(hsp70l:il4-6XHIS)*^{md74}	This paper	N/A
Mice: *BALB/c-Il4ratm1Sz/J*	Noben-Trauth et al., 1997, Jackson Laboratory	Stock No: 003514
Mice: *C57BL/6N*	MDC animal facility	N/A
Oligonucleotides		
See Table S1		N/A
Recombinant DNA		
myl7:RFP	This paper	N/A
myl7:il4rΔC-RFP	This paper	N/A
myl7:mKate-GR	This paper	N/A
Software and Algorithms		
Fiji/ImageJ	NIH	https://fiji.sc/
Imaris	Oxford Instruments	https://imaris.oxinst.com/
Prism	GraphPad Software	https://www.graphpad.com/scientific-software/prism/
FlowJo	BD (Becton, Disckinson & Company)	https://www.flowjo.com/solutions/flowjo

RESOURCE AVAILABILITY

Lead Contact

Further information and requests for resources and reagents should be directed to and will be fulfilled by the Lead Contact, Suphansa Sawamiphak (Suphansa.Sawamiphak@mdc-berlin.de).

Materials Availability

Plasmids and zebrafish lines generated in this study are available upon request.

Data and Code Availability

Raw data described in this study are available upon request.

EXPERIMENTAL MODEL AND SUBJECT DETAILS

Animal husbandry was performed under standard conditions, and experiments were conducted in accordance with institutional (Max Delbrück Center for Molecular Medicine), State (LAGeSo Berlin), and German ethical and animal welfare guidelines and regulations. Sex of zebrafish and mice cannot be determined at the developmental stages considered in this study. Animals were randomly assigned to experimental groups.

Zebrafish

All zebrafish experiments were performed on larvae up to 5 dpf. Previously established transgenic zebrafish lines used for this study include *Tg(myl7:Cre-ERT2)*^{pd12} (Kikuchi et al., 2010), *Tg(myl7:mKate-CAAX)*^{sd11} (Lin et al., 2012), *Tg(myl7:H2B-GFP)*^{zf52} (Mickoleit et al., 2014), *Tg(myl7:GAL4)*^{s740} (Sawamiphak et al., 2017), *Tg(actb2:loxP-DsRed-loxP-dnstat3 EGFP)*^{s928} (Fang et al., 2013), *TgBAC(csf1ra:GAL4-VP16)*^{i186} (Gray et al., 2011), *Tg(UAS-E1B:NTR-mCherry)*^{c264} (Davison et al., 2007), *Tg(kdrl:Hsa.HRAS-mCherry)*^{s896} (Chi et al., 2008), *Tg(myl7:GFP)*^{f1} (Burns et al., 2005), *Tg(fli:nls-mcherry)*^{ubs10} (Heckel et al., 2015), *Tg(wt1b:EGFP)*^{li1} (Perner et al., 207). To generate the *Tg(hsp70l:il4-6XHIS)*^{md74} line, we first amplified *il4* open reading frame and added 6xHIS epitope

CellPress
OPEN ACCESS

sequence to its C terminus by PCR from a cDNA library generated from 54 hpf zebrafish embryos. The *il4-6xHIS* fragment was then cloned downstream of a *hsp70l* promoter in a vector containing a *cryaa:Cerulean* expression cassette and I–SceI recognition sites. The construct was injected into one-cell stage embryos together with I-SceI meganuclease to enable genomic integration of the transgene. Injected embryos were sorted for Cerulean expression in the lens and raised to adulthood. Identified founders were outcrossed and offspring were raised and expanded.

Phenylthiourea (PTU) was applied to zebrafish starting from 1 dpf to block skin pigmentation.

Mice

BALB/c-*Il4ra*^{tm1Sz}/J (Noben-Trauth et al., 1997) mice were obtained from the Jackson Laboratory. Mice were genotyped by PCR with three primers (Il4ra_wt: TGTGGGCTCAGAGTGACCAT; Il4ra_mut: CCAGACTGCCTTGGGAAAAG; Il4ra_common: CAGGGAA CAGCCCAGAAAAG) which leads to amplification of 441 bp (wild-type allele) and 247 bp (mutant allele) DNA fragments. Postnatal (P0) C57BL/6N mice were used to obtain cardiomyocytes for cell cultures.

METHOD DETAILS

Generation of expression constructs

To generate the dominant negative form of zebrafish *il4r*, we amplified *il4r* lacking the cytoplasmic domain (*il4rΔC*) from a zebrafish cDNA library and cloned it downstream of *myl7* promoter in a pTol2 vector containing RFP using NheI and NcoI sites. Primers used are NheI-kozak-il4r.F: GATTGCTAGCGCCGCCACCATGAAGTTCAATGTTTCGTTT and NcoI-il4rdeltaC.R: GACACCATGGCC AAAAAACAGATGAAGGTCAT

Zebrafish *GR* (*zGR*) was amplified from PCS2+zGRa plasmid (Schaaf et al., 2008). The *zGR* gene fused to a sequence encoding Gly-Gly-Gly-Gly-Ser linker sequence and *mKate* was then inserted downstream of *myl7* promoter in the pTol2 vector using Cold Fusion Cloning Kit (System Biosciences). To generate the *myl7:RFP* construct, the *myl7* promoter and the RFP coding sequence were amplified and cloned into pTol2 vector using the Cold Fusion Cloning Kit (System Biosciences). Zebrafish embryos at one-cell stage were injected either with *myl7:mKate-GR, myl7:il4rΔC-RFP, or myl7:RFP* constructs. Each Injected fish were live imaged at day 3 and day 5. Cardiomyocyte proliferation was analyzed at 5 dpf. Apoptosis of cardiomyocytes was analyzed at 3dpf.

Gene expression by heat-induction and treatments with drug and neutralizing antibody

For heat induction of *il4-6xHis* expression, embryos were transferred into a water bath preheated at 38°C and kept at this temperature for 1.5 h. Larvae were bathed with 100 μM dexamethasone (Sigma), or 10 μM miferpristone (Sigma), plus 0.5% DMSO in Danieau's medium (58 mM NaCl, 0.7 mM KCl, 0.4 mM $MgSO_4 \cdot 7H_2O$, 0.6 mM $Ca(NO_3)_2$, 5 mM HEPES in water) at desired stages and for specific periods of time as indicated in the text. A solution of 0.5% DMSO in Danieau's buffer was used as control.

To activate Cre-ERT2, 1 dpf old zebrafish embryos were treated with ethanol-stocked 4-hydroxytamoxifen (4-OHT, Sigma) diluted in Danieau's buffer to a final concentration of 6 μM. After 24 h drug was washed out and embryos were kept in fresh Danieau's solution until 5 dpf.

Neutralizing antibody for IL4 (IL4-nAB) (Novus Biological, MAB204) was reconstituted at 0.5 mg/ml in PBS, and 2 μl (10 μg/ml) IL4-nAB was injected intrapericardially. A solution containing 10 μg/ml anti-6X-HIS antibody (Invitrogen, MA1-21315) in PBS was injected as control.

Stress treatment

4 dpf larvae were shaken for periods of 1 h duration at 300 rpm, alternated by 1 h-long intervals without shaking. The whole treatment lasted 16 h and was performed overnight. Control larvae were maintained in similar conditions, but in the absence of shaking. Afterward, larvae were stored in TRIzol at −80°C for RNA extraction, or fixed with 4% paraformaldehyde (PFA) for 2 h at room temperature for immunostaining.

Immunofluorescent and TUNEL staining

Larvae were fixed with 4% PFA + 0.3% triton at 4°C overnight, washed with PBS buffer containing 0.3% (V/V) Triton (PBST). An incision in the pericardium was performed to allow best accessibility of antibodies to the heart. Larvae were then kept in 100% methanol at −20°C for at least 2 h before proceeding to staining. To improve antibody penetration, larvae were incubated with a 1:20 dilution of Trypsin-EDTA (500 BAEE units, Sigma, T4200) in PBST on ice for 35 min followed by antigen retrieval with 150 mM tris-HCl, pH 9 at room temperature for 5 min and then at 70°C for 15 min. Then, larvae were incubated at room temperature for 1 h in blocking buffer (PBS supplemented with 0.3% (V/V) Triton X-100, 1% DMSO, 5% (v/v) goat serum, 1% (w/v) bovine serum albumin (BSA)), followed by primary antibodies diluted in blocking buffer for 72 h at 4°C. After washing with PBST, samples were incubated with Alexa Fluor 488 Goat Anti-chicken (1:1000, ThermoFisher, A10262), Alexa Fluor 647 anti-mouse (1:500, Cell Signaling, 4410S), Alexa Fluor 555 Anti-rabbit (1:750, Cell Signaling, 4413) in blocking solution for 48 h at 4°C, washed with PBST and mounted in Fluoromount aqueous mounting medium (Sigma) for imaging. Primary antibodies are chicken anti-GFP (1:1000, ThermoFisher, A10262), rabbit polyclonal RFP (1:500, MBL, PM005), and mouse Anti-Proliferating Cell Nuclear Antigen (PCNA) (1:300, Dako, M0879).

Cardiomyocyte apoptosis was detected by the TdT-mediated dUTP Nick-End Labeling (TUNEL) technique using a Click-iT TUNEL Alexa Fluor 647 kit (Invitrogen, C10247) according to manufacturer's protocol. Briefly, fixed larvae were incubated in TdT reaction at 37°C for 3 h followed by incubation in the Click-iT reaction at room temperature and protected from light for 1 h. For positive control, larvae were treated with DNase I solution for 30 min at room temperature. Immunostaining using anti-GFP and anti-RFP antibodies, described above, was performed to label cardiomyocyte nuclei.

Image analyses

To quantify proliferating and apoptotic cardiomyocytes, all single-plane images from confocal stacks that covered the entire cardiac ventricle or atrium were analyzed. Cells showing PCNA-labeled nuclei that were co-localized with H2B-GFP were counted in ImageJ. Total cardiomyocyte numbers and endocardial cell numbers were quantified using Imaris software (Oxford Instruments). Epicardial cell numbers were counted in ImageJ. Ventricular volume was calculated using Volumest plugin in ImageJ. Trabecular and compact wall cardiomyocytes were counted from confocal z stacks with 10 μm intervals. A total thickness of 40 μm of the ventricle was quantified for each heart. Both membrane and nuclear makers were used to distinguish individual cardiomyocytes. Cell volume was quantified using ImageJ.

Mouse histological and immunofluorescence analyses

Neonatal (P0) hearts were dissected, rinsed with PBS, and fixed overnight with 4% PFA in PBS at 4°C. After washing in PBS, hearts were embedded in paraffin. 7 μm-thick sections were used for immunofluorescence staining of the cardiomyocyte marker Tnnt2 (Anti-Troponin T2, Cardiac Type antibody, Abcam, ab33589), and proliferation marker Ki67 (Anti-Ki-67 Antibody, Millipore, AB9260). After deparaffinization and rehydration, antigen retrieval was done with citrate buffer (10 mM citric acid, 0,05% Tween 20, pH 6) 15 min in a microwave. Then sections were blocked for 1 hour at room temperature with a solution of 3% BSA, 5% goat serum, 0.3% Tween 20 in PBS. Sections were incubated overnight at 4°C with primary antibodies (1:200 Tnnt2, 1:100 Ki67) in blocking solution. Subsequently, sections were rinsed and incubated with Alexa Fluor-conjugated secondary antibodies (1:500 anti-mouse Alexa647, Cell Signaling 4410S, 1:500 anti-rabbit Alexa488, Cell Signaling 4412) for 1 hour at room temperature. Finally, sections were treated with 1% hydrogen peroxide for 20 min at room temperature. Mounted sections were examined with a Zeiss LSM880 NLO confocal microscopy system. 25000 square micron areas from each section were used for quantification of $Tnnt2^+$/$Ki67^+$ double positive cells. Masson's trichrome staining was performed according to the manufacturer's instruction (Roche 860-031). Ventricular wall and total ventricular areas were measured with ImageJ software.

Wheat germ agglutinin (WGA) staining was performed simultaneously with secondary antibodies step of immunofluorescent staining. Slides were incubated overnight at 4°C with 1:200 dilution of WGA (WGA-conjugated CF555, Biotium, 29076-1). Cardiomyocyte density was determined by counting of $Tnnt2^+$/WGA^+ double positive cells. Four fields of each section were examined for quantification. In order to quantify cell size; cardiomyocyte cross sectional area was measure in ImageJ. One hundred twenty cardiomyocytes with a nucleus centrally located were analyzed per each experimental group.

In situ hybridization

In situ hybridization for the assessment of *il4*, *il4r, ifng1,* and *ifngr1* expression was performed as described earlier (Sawamiphak et al., 2014). Probes were generated by PCR amplification of a 54 hpf cDNA library. Primers used were:

IL4.F: ATGAAGACCTGAAGATCTCAACATCTGGATACATC
IL4R.F: GTTTCGTTTGCGAATAGGGAAGCAG
T7IL4.R: TAATACGACTCACTATAGGGTTATGTCCTTTGAGCCGAG T7IL4R.R: TAATACGACTCACTATAGGGGAGCAGTGGTGA AATGAACTG
ifng1.F: ATGATTGCGCAACACATGATGGGCT
T7ifng1.R: TAATACGACTCACTATAGGGACCTCTATTTAGACTTTTGC
ifngr1.F:
GTTGGATACAAACTCTGTGGTAATAATAATGCGGATATTGATCTGTC
T7ifngr1.R: TAATACGACTCACTATAGGGGAAAGCTCATGTACGCCTCG

Cardiac contractility measurements

5 dpf larvae, which were either daily exposed to 38°C to induce *il4-6xHis* expression or dexamethasone treated from 2 to 5 dpf, were embedded in 2% low-melting-point agarose. The ventricles were imaged with a transmitted light microscope equipped with a 40X objective and a high-speed camera (Ximea). 10 s-long movies were acquired at 300 frames per second.

To calculate diastolic and systolic speed, areas of the heart at the end of a diastole and of a systole were measured in Fiji. Area change by time was calculated as diastolic or systolic speed. Width of the ventricle at the maximum ventricular diastole ($width_{VD}$) and ventricular systole ($width_{VS}$) were measured in Fiji and ventricular fractional shortening (FS) was calculated as [100 x ($width_{VD}$ – $width_{VS}$)/$width_{VD}$]. Ejection fraction (EF) was evaluated from ventricular volume at the end of diastole ($volume_{VD}$) and systole ($volume_{VS}$). We first measured ventricular width and length at the end of diastole ($width_{VD}$ and $length_{VD}$) and systole ($width_{VS}$ and $length_{VS}$) using Fiji. Then the $volume_{VD}$ and $volume_{VS}$ were calculated as [π x $length_{VD}$ x $width_{VD}^2$)/6]

and [π x $length_{VS}$ x $width_{VS}^2$)/6], respectively. Finally, EF was calculated as [100 x ($volume_{VD}$ – $volume_{VS}$)/$volume_{VD}$] (Yalcin et al., 2017).

Real-time PCR

5 dpf larvae were treated with 100 μM dexamethasone for 2 h, or exposed to 38°C for 1.5 h to induce *il4-6xHis* expression, followed by 2 h recovery at room temperature. Next, hearts were dissected and collected in PBS immediately and then stored in TRIzol at −80°C until usage. Total RNA was isolated from pooled whole zebrafish larvae (50) or isolated hearts (250-300) with TRIzol reagent (Life Technologies) according to manufacturer's instructions. 2 μg of RNA was reverse-transcribed using the SuperScript III First Strand Kit (Life Technologies). Real-time PCR was performed using Luna Universal qPCR Master Mix (New England BioLabs) and run on a StepOnePlus Real-Time PCR System (Applied Biosystems). Samples were analyzed using $2^{-\Delta\Delta Ct}$ method (Gibson et al., 1996). The housekeeping gene *gapdh* was used for normalization.

PRIMERS USED IN THE EXPERIMENT ARE

bcl2l1: forward GCAGATTGTGTTATGGGTATGAGC, reverse GGTTGCAGGGGTAGTTCCTC
c-myc: forward GGCAGCGATTCAGAAGATGAAG, reverse CCGTCTCGTGCCTTTTCTGT
cyclinD1: forward GCCAAACTGCCTATACATCAG, reverse TGTCGGTGCTTTTCAGGTAC
gapdh: forward GTGGAGTCTACTGGTGTCTTC, reverse GTGCAGGAGGCATTGCTTACA
gata3: forward CCTGCGGACTTTACCACAAG, reverse ACAGTTTGCGCATGAGGTC
il4: forward CTGTTGGTACTTACATTGGTCCCC, reverse AGTGTCCTGTCTCATATATGTCAGGT
il4r: forward AGCAGCCAGCAGACTGAAAT, reverse ATGGGATCGTCACAAAGTGCT
il13ra1: forward GCATGTCAGAGCTTCCTCCG, reverse AGACCTTGTTGGTGGCAACT
il13ra2: forward GAGCGATGGAGGAGTGTTCG, reverse ATTGGTACAGGCGCACTTCA
socs1a: forward GCGCTCTGAGGAAACCTCTA, reverse GAGACTCATCGGTCGTTTTAGT
stat3: forward GGACTTCCCGGACAGTGAG, reverse ATCGCTTGTGTTGCCAGAG

Mouse cardiomyocyte isolation, culture and immunocytochemistry

Postnatal day 0 C57BL/6N pups were used for cultivation of neonatal cardiomyocytes which were prepared with slight modifications according to an established protocol (Fu et al., 2005). After dissection of hearts, cells were dissociated by repeated enzymatic digestion (0.08% trypsin in PBS, GIBCO 15090046; plus 50 μg/ml DNaseI, Roche 10104159001) and cultivated in DMEM, high glucose, GlutaMAX supplement (GIBCO, 31966021) supplemented with 10% fetal calf serum (GIBCO, 10270-106) and Penicillin-Streptomycin (10.000 U/ml) (Thermo Fisher, 15140122) at 37°C in 95% air/5% CO_2. Cells were plated (100 μl suspension per coverslip) on glass coverslips (12 mm in diameter) pre-coated with 10 μg/ml bovine plasma fibronectin (Thermo Fisher, 33010-018) to obtain a dense monolayer of cardiomyocytes (the density varied from preparation to preparation, range $0.6x10^5$ to $3.1x10^5$ per coverslip, due to a variable contamination with erythrocytes). After attachment, additional medium was added and cells were allowed to grow for additional 24 hours. Then, cells were treated with ethanol as a vehicle control, 100nM dexamethasone (Sigma, D4902), 10 ng/ml recombinant murine IL4 (PeproTech, 214-14), or dexamethasone (100 nM) plus recombinant IL4 (10ng/ml) in serum free medium for 24 hours. Cells were incubated with 2 μM EdU for the last 12 h before fixation.

After treatments, cells were washed with PBS and fixed with 4% PFA in PBS followed by 20 minutes permeabilization with Triton X-100 (0.1%). Cells were then incubated with blocking solution (PBS supplemented with 1% BSA, 5% goat serum, and 0.1% Triton X-100) for 1 hour, followed by incubation with primary antibody (1:300 mouse cardiomyocyte marker Tnnt2, Anti-Troponin T2, Abcam, ab33589) overnight at 4°C. After washing, cells were incubated with Alexa Fluor secondary antibody (1:1000 goat anti mouse Alexa488, cell signaling 4408S). EdU staining was performed using Click-iT EdU imaging kit (Thermo Fisher, C10640) according to the manufacturer's protocol. Cell nuclei were stained with DAPI (1 μg/ml). Mounted coverslips were imaged with a Zeiss LSM880 confocal microscopy system. Analysis was performed using ImageJ software.

Flow cytometry and polyploidy analysis

Nuclear ploidy was determined using flow cytometry. Dissociated cardiomyocytes were fixed with 4% PFA in PBS for 10 min. Cells were then incubated with blocking solution (PBS supplemented with 2% BSA) for 1 hour, followed by incubation with primary antibody (1:200 mouse cardiomyocyte marker Tnnt2, Anti-Troponin T2, Abcam, ab33589) for 2 hours at room temperature. After washing three times with PBS, cells were incubated with Alexa Fluor secondary antibody (1:500 goat anti mouse Alexa488, Cell Signaling 4408S). The nuclei were stained with DAPI (1 μg/ml). Intensity of DAPI fluorescence in nuclei of Tnn2-positive cardiomyocytes was measured with a flow cytometer (FACS Aria II, BD Biosciences), and analysis was performed using FlowJo 10.6.2 software.

QUANTIFICATION AND STATISTICAL ANALYSIS

Statistical significance, with the exception of qPCR data and data shown in Figure S7B, was determined using two-tailed Student's t tests in Graphpad Prism. For data shown in Figure S7B one-sample Student's t tests were used. When performing multiple comparisons, p values were corrected using the Holm-Bonferroni method.

For real-time PCR data, statistical significance was determined with one-sample Student's t tests, and p values were adjusted for multiple comparisons using the *Benjamini-Hochberg* procedure. Outliers in real-time PCR datasets were removed after detection with Dixon's test.

Differences were considered statistically significant if $p < 0.05$. Unless otherwise stated, n indicates the number of animals used for experiments.